

Risk Assessment of COVID Infection by Respiratory Droplets from Cough for Various Ventilation Scenarios Inside an Elevator: An OpenFOAM based CFD Analysis

Riddhideep Biswas, Anish Pal, Ritam Pal, Sourav Sarkar*, Achintya Mukhopadhyay

Department of Mechanical Engineering, Jadavpur University, Kolkata-700032, India

*corresponding author: souravsarkar.mech@jadavpuruniversity.in

Abstract

Respiratory droplets exhaled during speaking, coughing or sneezing have been responsible for the spread of the ongoing Covid-19 pandemic. The droplet dynamics depend on the surrounding air velocity, temperature and relative humidity. Droplets evaporate to form aerosols which contain the disease spreading virus. In a confined space like an elevator, the risk of transmission becomes higher when there is an infected person inside the elevator with other individuals. In this work, a numerical study is carried out in a 3D domain resembling an elevator using OpenFoam. Different modes of air ventilation are considered inside the elevator and the impact of these air circulations on droplet dynamics is investigated. The scenario of the opening of elevator door and the passenger leaving the elevator has also been considered in order to simulate a real life condition. A pedantic analysis of certain risk assessment factors and remedial measures to be adopted has been performed which include the number of aerosols present in the zone of 0.8 to 1.8 m, the radial spread of the suspended droplets around the mouth of the infected person. From these factors, the safe condition can be understood. The time period up to which the elevator will be risk prone has also been investigated in case the person coughs just before leaving the elevator. After conducting these studies, the quiescent environment has been found out to be the most dangerous whereas ventilation with an exhaust fan is the safest.

Keywords: Respiratory droplets, elevator, ventilation, virusol, risk factor, OpenFOAM

I. Introduction

The ongoing pandemic of Covid-19 has caused an immense loss of lives as well as shattered the global economy, the entire world still suffering from its excruciating shackles. The transmission of Sars-Cov-2 has been responsible for this pandemic and it has been established that the virus spreads through respiratory droplets^{1,2}. Respiratory droplets are exhaled from the mouth or nose during speaking, coughing or sneezing. The conditions of speaking, coughing or sneezing can be differentiated with the help of droplet size and velocity spectra and exhalation velocity of jet from the mouth³. The respiratory droplets are laden with salt and proteins which contain the virions. Whenever respiratory droplets are expelled from the mouth by coughing or sneezing, it is expected that the droplets will follow a projectile motion and eventually settle on the ground. But during coughing, a turbulence is generated by the air puff which takes the responsibility of carrying the droplets an appreciable amount of distance³. While travelling the distance, the droplet undergoes evaporation which reduces the size of the droplets thereby helping them to cover more distance. Redrow et. al. modelled the evaporation and dispersion of cough jet droplets considering sputum for the first time and showed that the human cough includes a turbulent air puff⁴. Wei et. al showed that the droplet spread gets enhanced by the presence of turbulent air jet⁵. Kwon et.al performed experiments involving particle image velocimetry to study the initial velocity distributions from coughing and sneezing⁶. Li et.al computationally modelled the evaporation of cough droplets employing the multi-component Eulerian-Lagrangian approach in inhomogeneous humidity condition⁷. Johnson et.al performed experiments with Aerodynamic Particle Sizer in order to obtain the aerosol size distribution which gets expelled from the mouth during coughing⁸. Dbouk and Drikakis have conducted a computational study to investigate the transport, dispersion and evaporation of respiratory droplets produced from a human cough⁹. Wang et. al. performed flow visualization and particle image velocimetry to understand the motion of the droplets and utilised those results to establish a physical model for investigating the trajectories of the droplets expelled by cough¹⁰. Pendar et.al conducted a wide range study of the velocity distribution, expelled angle and the size of the droplets released from the mouth in order to determine the correct social distance guidelines for different conditions¹¹. If a person is present in an open area like a school ground or market place, the risk of the disease transmission depends on wind velocity due to the available space between two persons. Feng et.al carried out a numerical study to investigate the effects of wind and relative humidity on the transportation of respiratory droplets in an outdoor environment and it

was found that in presence of wind, the microdroplets can be transported to larger distances¹². Li et.al performed numerical study on dispersion of cough droplets with non-volatile components in a tropical outdoor environment and the dispersion was influenced by the relative humidity and wind speed¹³.

In an open space, it has been observed from the above literatures that the wind speed affects the spread of the droplets but the situation becomes alarming in a confined space like an elevator or a cabin where the environment is enclosed and if a person coughs, the droplets will remain inside the space for an appreciable amount of time. Liu et.al performed a laboratory study to investigate the expiratory airflow and particle dispersion in a stratified indoor environment¹⁴. Cheng et.al investigated the trajectories of large respiratory droplets in indoor environment under different relative humidity¹⁵. Yang et.al carried out a computational study to capture the dispersion of pathogen-laden respiratory droplets in an enclosed environment like crowded bus¹⁶. Yan et.al employed the Lagrangian-based Wells-Riley approach to assess the risk of airborne disease infection in an airliner cabin¹⁷. Yan et.al numerically investigated the thermal effects of human body on the evaporation and dispersion of cough droplets in an enclosed environment¹⁸. Sen performed a numerical study to investigate the evaporation and transmission of cough droplets in a confined space like elevator considering different scenarios such as varying the air ventilation systems, number of persons inside the elevator, direction of ejection, relative humidity and temperature¹⁹. Dbouk et.al showed how the modifications in ventilation systems in confined spaces can influence the transmission of airborne virus²⁰. Agrawal et.al has worked on the reduction of the risk associated with cough cloud in a closed space by modifying the ventilation systems²¹. All these works have paid attention to the ventilation systems but none of them have studied the effect of opening of an elevator door on the spread of the aerosols or the droplets and the risk to which another person will be exposed when he tries to board the elevator after the door opens. Moreover, in these works, pure water droplet has been considered which does not resemble real scenario where the droplet is pathogen laden. The droplets contain non-volatile salts in some specific proportions and these salts contain the pathogen. A salt laden droplet will have thermophysical properties different from that of pure water droplet, and the thermophysical properties will constantly change with evaporation, unlike pure water. This difference and constant change in thermophysical properties will cause a difference in the mass transfer number and hence the evaporation rate, ultimately manifesting itself in a difference in the overall droplet dispersion and trajectory than that of pure water. So, in order to mitigate the above stated problem and to make the simulations and their corresponding results more realistic, our work has implemented this salt model of droplet along with droplet evaporation. In addition, a systematic comparison of the risk of infection from different designs of ventilation along with the safety measures to be adopted in each of the designs has been carried out in this work.

In confined spaces, the ventilation plays a significant role which has been highlighted in the existing literature. When the droplets are inside the enclosed space, they will undergo evaporation which will transform them into aerosol and they can remain suspended in the air for longer periods of time. Several works have been reported recently where the aerosol route of virus transmission has been supported with enough evidences^{9,22-24,25}. The aerosol size is generally considered less than 10 micron which helps them to remain suspended in the air for longer periods of time and from the recent works, it can be concluded that the aerosol constitutes the virions which are responsible for the disease transmission²⁶. So, when a person coughs or sneezes in a confined space like an elevator, the aerosol will remain in the space until it is forced out or it gets any opening to discharge outside. This implies that when an elevator door will open for the passenger who is waiting outside, the passenger will be exposed to a high-risk situation in the elevator if the former passenger inside the lift has just coughed before opening of the door. Face masks may work as a protective gear up to a certain extent but there are limitations. Akhtar et.al performed droplet flow visualization experiments to test the effectiveness of five different masks and it was found that except for the N-95 masks, all the other masks showed some amount of droplet leakage²⁷. Dbouk et.al has also worked on the effectiveness of masks to reduce the droplet transmission²⁸. The risk assessment of such situations is necessary as it will help to understand the safe time interval between stopping of the elevator and boarding it. Moreover, the assessment can also give information regarding the safe distance which must be maintained from the infected passenger inside the elevator.

In this work, a 3D geometry of an elevator has been considered. A passenger is present inside that elevator without a face-mask and the passenger is coughing. Different ventilation conditions of the ambience have been investigated considering both quiescent environment and forced circulation of air in the domain. The dispersion and evaporation of the droplets (including non-volatile components) has been investigated in each of the cases. The situation is such

that the person has boarded the elevator and before alighting from the elevator, the person coughs. The beleaguered person waiting outside to board the elevator will be oblivious to the threat that looms inside the elevator. Our paper focuses on the risk assessment of this situation for various ventilation conditions along with suggestions of safety measures.

II. Problem Formulation

A. Geometry

The computational domain consists of an elevator having a capacity of 5 persons which is portrayed in Fig. 1 (a), describing its details. The dimension of the elevator is 1.2 X 1.2 X 2m, which is a typical size of an elevator in a residential building complex or small enterprises. Investigation of a smaller size elevator is necessary as the risk associated with a smaller confined space is higher. At the top of the elevator, a circular mounting of 0.6 m diameter is provided. This top circular mounting is subjected to conditions specific to each particular scenario, as illustrated further in the Initial and Boundary Conditions section as well as in Table 1. This top mounting is a very important part as by altering the boundary conditions on this mounting, the various ventilation situations inside the elevator are realized. In the present study, various boundary conditions representing a fan or an exhaust fan at the top opening have been presented as different scenarios investigated. The ventilation slots, 3% of the platform area, have been provided at the bottom of side walls of the elevator (complying with the European EN-81-1 code²⁹). In Scenario 6, the door of the elevator is opened, as discussed later. In order to mimic the real-life gradual opening of a sliding elevator door, the door in our geometry is partitioned into six panels. Figure 1(a) also shows the entire door, clearly depicting each of its partitions. In Scenario 6, the entire door is not opened at once, but the partitions are opened one by one, following a particular relation and in this way, the entire door is opened in steps, thus closely simulating a real-life opening of an elevator door. Instead of incorporating a human manikin, the features of the passenger namely, the head, face, mouth and remaining body parts have been represented with rectangular boxes, whose dimensions correspond to those of a typical human being in the standing posture, to reduce the complexity and the computational cost and time. Also, since our area of focus in the domain is far away from the passenger, implementation of a geometry that corresponds to an actual human being will have no effect on our desired zone of interest. The passenger height is taken as 1.75m (the height of the mouth being 1.56 m from bottom) (Chillón et al.³⁰). Figure 1 (b) shows the isometric view of the passenger in the domain, which also shows the position of the passenger relative to the elevator walls. The mouth of the passenger, from which the cough droplets are injected, has been modelled as a rectangular-shaped aperture having a width of 40 mm and an aspect ratio of 8 (Chillón et al.³⁰), as shown in Fig. 1 (c). Various scenarios have been studied to understand the effect of air flow in the surrounding environment on transmission and evaporation of droplets, injected into the domain by coughing of the passenger. Droplets generated due to the coughing of the passenger would travel in the domain depending on the preponderant velocity field. Certain number of droplets could turn into aerosols depending on the prevailing temperature and humidity. A fraction of droplets might escape, a few of them may stick on the various surfaces within the elevator, while the remaining ones will remain suspended in the domain for extended periods – the last ones being of major concern to us.

B. Mathematical Model

An Eulerian-Lagrangian model has been implemented for this numerical study. Air, the carrier fluid is modelled in the Eulerian frame. For the carrier bulk multiphase fluid mixture, the continuity (equation 1)^{19,31} and the compressible multiphase mixture Reynolds-averaged Navier–Stokes equations (equation 2)^{19,31} in conjunction with the $k - \omega$ turbulence model in the shear-stress-transport formulation (equations 3-15)³² has been employed. Droplets that are injected into the domain due to coughing are solved as discrete particles in a Lagrangian frame of reference. The droplets move around depending on the prevailing velocity field of the air and undergo evaporation while they traverse the domain. The droplets and moist air at the time of ejection from the mouth can be considered to be at the same temperature as that of the body temperature. However, as the cloud of droplets intermingles with ambient air, it entrains a significant quantity of ambient air after which the cloud temperature would effectually be the same as ambient temperature (Agarwal and Bhardwaj, 2020). However, evaporation still continues (as long as the volatile component of the droplet exists), and the energy needed for the phase change to occur is obtained from the droplet and the surroundings (equation 24)¹⁹. This reduces the temperature of the droplet below the ambient dry bulb temperature up to wet bulb temperature and hence the droplets reach the wet bulb temperature. The driving force for

the occurrence of evaporation of water is the difference of partial pressure of water vapour at the surface of the droplets and partial pressure of water vapor in the air surrounding the droplets (equation 27)¹⁹. The rate of evaporation depends upon the mass transfer coefficient determined from the Sherwood number (equations 27, 28). Sherwood number, again, is dependent upon the droplet Reynolds number (equation 29)³¹ based on the Ranz-Marshall correlation (equation 28)^{33,34}. The droplet is considered to be a mixture of salt and liquid water (99% water and 1% NaCl by wt.). As the droplets evaporate to lose the volatile liquid mass into the ambient (equation 20)¹⁹ and their diameter decreases, the mass fraction of its components change (equations 32, 33) and finally the droplet fully evaporates i.e. becomes fully devoid of the volatile liquid water component, forming droplet nuclei. The droplet properties used in the governing equations are a function of the properties of liquid water and salt as well as their respective mass fractions (equations 34, 35). The continuous change in the mass fractions of the components owing to the evaporation of the droplets has been taken into account (equations 32, 33). Hence, to incorporate this salt model of the droplets (equations 31-36), modifications has been made in the source code of the reactingParcelFoam solver of OpenFOAM. The Ranz-Marshall model has been implemented to calculate the Nusselt number (equation 18)^{33,34} and Sherwood number (equation 28)^{33,34}, to solve the droplet heat transfer (equation 24)¹⁹ and mass transfer (equation 27)¹⁹. The droplet temperature is obtained by solving the energy conservation equation, as discussed below (equation 24)¹⁹. The evaporative cooling is modelled by taking into account the energy transfer from the bulk phase into Lagrangian phase (16, 17)¹⁹. The position and the velocity of the droplets are obtained by applying Newton's second law of motion on the droplets and the forces considered here are gravity, buoyancy, lift and drag (equations 23, 26)^{19,31}. The relevant gas phase and particle phase transport equations with appropriate closure relations are given below.

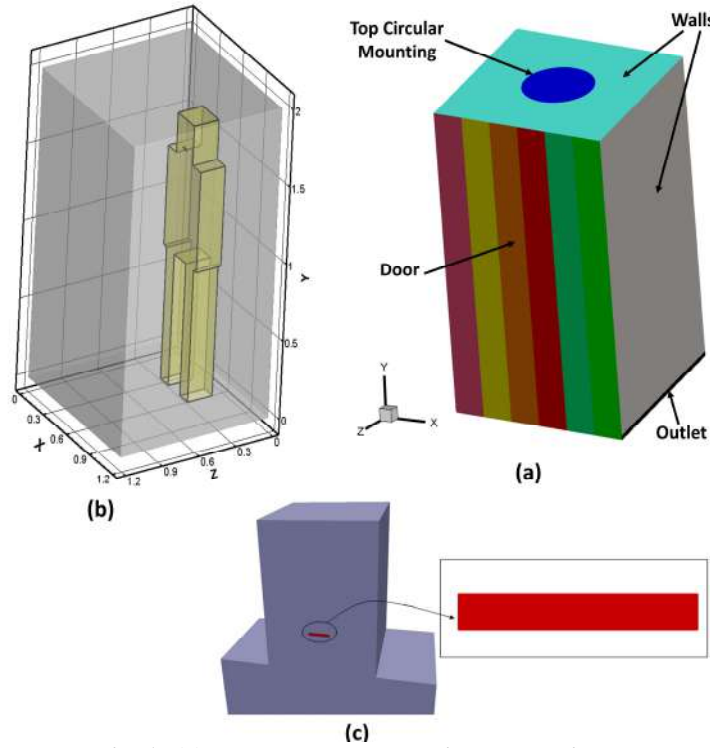


Fig. 1: (a) The whole computational domain.
(b) Isometric view of the passenger in the domain.
(c) Mouth of the passenger modelled as a rectangular aperture.

Governing Equations for the Eulerian (Gas) Phase.

Continuity equation
$$\frac{\partial \rho}{\partial t} + \rho \nabla \cdot (\vec{u}) + \vec{u} \cdot \nabla(\rho) = 0 \quad (1)$$

Momentum equation $\rho \frac{\partial \vec{u}}{\partial t} + \rho(\vec{u} \cdot \nabla)\vec{u} = \nabla \cdot [-pI + \bar{\tau}] + \rho \vec{g}$ (2)

Closure equation for the momentum equation $\bar{\tau} = (\bar{\mu} + \bar{\mu}_t) (\nabla \vec{u} + (\nabla \vec{u})^T - \frac{2}{3}(\nabla \cdot \vec{u})\bar{I}) - \frac{2}{3}\rho k \bar{I}$ (3)

Transport equation for turbulent kinetic energy $\frac{\partial(\rho k)}{\partial t} + \frac{\partial(\rho u_j k)}{\partial x_j} = P - \beta^* \rho \omega k + \frac{\partial}{\partial x_j} \left[(\mu + \sigma_k \mu_t) \frac{\partial k}{\partial x_j} \right]$ (4)

Transport equation for turbulent energy dissipation $\frac{\partial(\rho \omega)}{\partial t} + \frac{\partial(\rho u_j \omega)}{\partial x_j} = \frac{\gamma}{\nu_t} P - \beta \rho \omega^2 + \frac{\partial}{\partial x_j} \left[(\mu + \sigma_\omega \mu_t) \frac{\partial \omega}{\partial x_j} \right] + 2(1 - F_1) \frac{\rho \sigma_{\omega 2}}{\omega} \frac{\partial k}{\partial x_j} \frac{\partial \omega}{\partial x_j}$ (5)

Turbulent kinetic energy production $P = \tau_{ij} \frac{\partial u_i}{\partial x_j}$ (6)

Reynolds stress tensor $\tau_{ij} = \mu_t \left(2S_{ij} - \frac{2}{3} \frac{\partial u_k}{\partial x_k} \delta_{ij} \right) - \frac{2}{3} \rho k \delta_{ij}$ (7)

Strain rate $S_{ij} = \frac{1}{2} \left(\frac{\partial u_i}{\partial x_j} + \frac{\partial u_j}{\partial x_i} \right)$ (8)

Eddy viscosity limiter $\mu_t = \frac{\rho a_1 k}{\max(a_1 \omega, \Omega F_2)}$ (9)

Weighted model constants $\phi = F_1 \phi_1 + (1 - F_1) \phi_2$ (10)

Blending function 1 $F_1 = \tanh(\text{arg} g_1^4)$ (11)

Argument for blending function 1 $\text{arg} g_1 = \min \left[\max \left(\frac{\sqrt{k}}{\beta^* \omega d}, \frac{500\nu}{d^2 \omega} \right), \frac{4\rho \sigma_{\omega 2} k}{CD_{k\omega} d^2} \right]$ (12)

Blending function 2 $F_2 = \tanh(\text{arg} g_2^2)$ (13)

Argument for blending function 2 $\text{arg} g_2 = \max \left(2 \frac{\sqrt{k}}{\beta^* \omega d}, \frac{500\nu}{d^2 \omega} \right)$ (14)

Constants $\left. \begin{aligned} \sigma_{k1} &= 0.85, \sigma_{w1} = 0.65, \beta_1 = 0.075 \\ \sigma_{k2} &= 1.00, \sigma_{w2} = 0.856, \beta_2 = 0.0828 \\ \beta^* &= 0.09, a_1 = 0.31 \end{aligned} \right\}$ (15)

Energy conservation equation $\rho \frac{\partial H}{\partial t} + \nabla \cdot [\rho \vec{u} H - \nabla(k_t T)] = Qd$ (16)

Energy transport from Eulerian to Lagrangian phase $Qd = \sum_{i=1}^{i=N} (\pi d_{d,i}^2 h (T - T_{d,i}))$ (17)

Ranz-Marshall correlation for Nusselt number $Nu = \frac{hd_d}{k_t} = 2.0 + 0.6Re_d^{0.5}Pr^{0.33}$ (18)

Prandtl number $Pr = \frac{c_p \mu}{k_t}$ (19)

Species transport equation as applied to turbulent flows $\frac{\partial(\rho f_v)}{\partial t} + \nabla \cdot [\rho \vec{u} f_v - \rho D_{eff} \nabla f_v] = m_v'''$ (20)

Closure term for the species transport equation $D_{eff} = D_{mol} + \frac{|\mu \bar{u}|}{\rho Sc_t}$ (21)

$Sc_t = 0.7$ (22)

Governing Equations for the Lagrangian phase (droplet properties and parameters subscripted by d)

Equation of motion of droplet $m_d \frac{du_d}{dt} = (\rho_d - \rho)g + \frac{C_d \pi \rho d_d^3}{8} |\vec{u}_d - \vec{u}| (\vec{u}_d - \vec{u}) + F_{lift}$ (23)

Energy-conservation equation, droplet phase $m_d C_{p,d} \frac{dT_d}{dt} = h \pi d_d^2 (T - T_d) + \frac{dm_d}{dt} h_{fg}$ (24)

Drag coefficient $C_d = \max \left\{ \frac{24}{Re_d} (1 + 0.15 Re_d^{0.687}); 0.44 \right\}$ (25)

Lift force $F_{lift} = \frac{2Kv^{0.5} \rho d_{ij}}{\rho_d d_d (d_{ik} d_{kl})^{0.25}} (\vec{u} - \vec{u}_d)$ (26)

Droplet evaporation term $\frac{dm_d}{dt} = \pi d_d^2 m_{wl} k_{mt} \left(\frac{p_{sat}}{RT_d} - X \frac{p}{RT} \right)$ (27)

Ranz-Marshall correlation for Sherwood number $Sh = \frac{k_{mt} d_d}{D} = 2.0 + 0.6Re_d^{0.5}Sc^{0.33}$ (28)

Droplet Reynold number $Re_d = \frac{d_d (\vec{u} - \vec{u}_d) \rho}{\mu}$ (29)

Schmidt number $Sc = \frac{\mu}{\rho D}$ (30)

Mass of nonvolatile component $m_d^s = Y_0^s m_d^0$ (31)

Mass fraction of nonvolatile component $Y_d^s = \left(\frac{m_d^s}{m_d} \right)$ (32)

Mass fraction of volatile component $Y_d^l = 1 - Y_d^s$ (33)

$$\text{Droplet density} \quad \rho_d = \frac{1}{\left(\frac{Y_d^s}{\rho^s}\right) + \left(\frac{Y_d^l}{\rho^l}\right)} \quad (34)$$

$$\text{Droplet heat capacity} \quad c_{p,d} = Y_d^s c_{p,s} + Y_d^l c_{p,l} \quad (35)$$

$$\text{Droplet diameter} \quad d_d = \left(\frac{6m_d}{\pi\rho_d}\right)^{1/3} \quad (36)$$

C. Initial and Boundary Conditions

The top circular mounting is assigned different conditions corresponding to different scenarios. Table 1 provided below elucidates this further. The two outlets provided at the bottom of the side walls are defined as pressure outlets with atmospheric pressure. All the walls and the boundary of the passenger are defined as walls with no slip velocity boundary condition. The door remains closed in all the Scenarios except Scenario 6, and hence in all these scenarios, the door is modelled as a wall. As discussed earlier, the door is partitioned into six divisions. In Scenario 6, where the door is opened, a pressure outlet boundary condition is applied to each division of the door when it remains open. By conducting numerical simulations, it has been inferred that the initiation time of the cough and air flow development in the domain has significant impact on the droplet kinematics. To eliminate this above stated bias and to make the situation more representative and generic, the cough is ejected in stages. The complete coughing phenomenon occurs in four stages. As depicted in Fig. 2, the coughing phenomenon commences at 1s and terminates at 4.12s. Each single cough occurs for 0.12s, injecting 1008 droplets of mass 7.7 mg with a velocity of 8.5 m/s normal to the mouth surface (Sen¹⁹). In each stream, the initial size distribution of the cough droplets follows the well-known Rosin-Rammler distribution or the Weibull distribution with a scale factor of 80 μm and shape factor of 8 (Sen¹⁹). The ambient temperature inside the elevator is 30°C. The passenger, assumed to be a symptomatic COVID infected patient, has a comparatively higher body temperature of 38.4°C. The continuous periodic inhalation and exhalation of the passenger has also been taken into account. The ambient pressure and relative humidity inside the elevator are atmospheric pressure (101325 Pa) and 50% respectively. The temperature of the air ejected out of the mouth during exhalation is assumed to be at the body temperature and its relative humidity is assumed to be 100% (Sen¹⁹). The injected cough droplets are also at the body temperature. The cough droplets are considered as a mixture of NaCl (salt) and water with initial mass fractions of 0.01 NaCl (solid) and 0.99 water (liquid)³⁵.

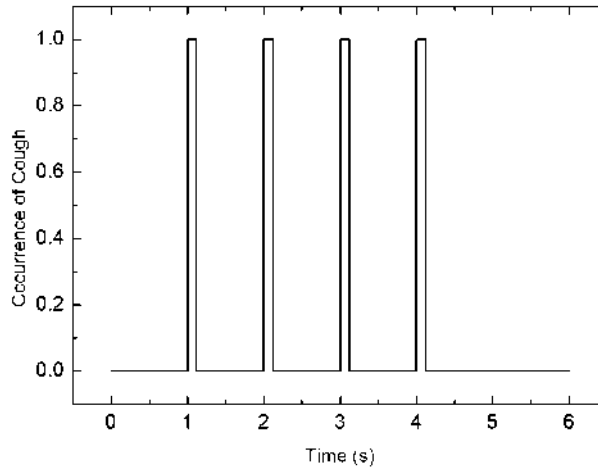


Fig. 2: The entire coughing phenomenon

D. Numerical Method

The OpenFOAM solver “reactingParcelFoam”, with necessary modifications to successfully implement the salt model as discussed earlier was employed to solve all the required partial differential equations. It is very important to state that all the thermophysical properties of the Eulerian and Lagrangian phases are functions of temperature. The Eulerian phase has been modelled as an ideal gas for its equation of state, and its transport is modelled using Sutherland’s law³⁶ for its viscosity based on the kinetic theory of gases, which is suitable for non-reacting gases. Finite volume methods have been employed to discretize the Eulerian phase. Second-order schemes have been employed for both time and space operators. Semi-implicit numerical schemes of second order have been employed for Lagrangian phase discretization.

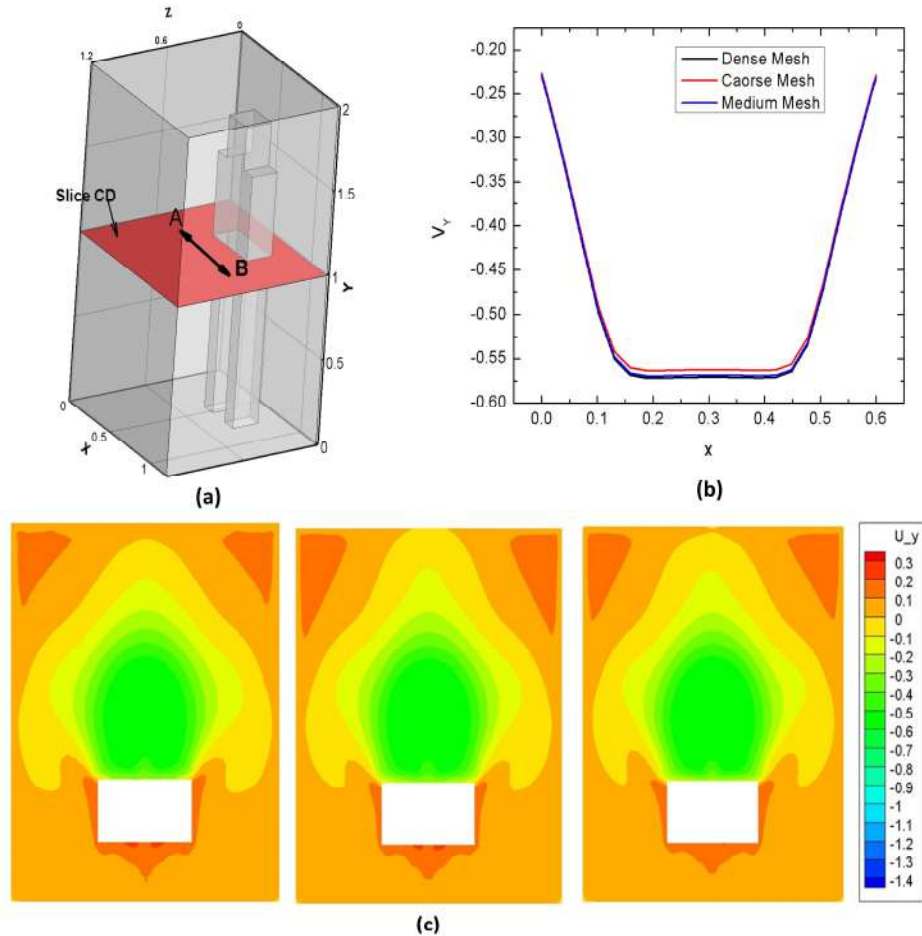


Fig. 3: (a) Location of slice CD and line AB
(b) Comparison of Velocity profile(V_y) of different mesh sizes at line AB.
(c) Comparison of velocity contours of different mesh sizes at slice CD for coarse, medium and fine mesh sizes respectively from left to right

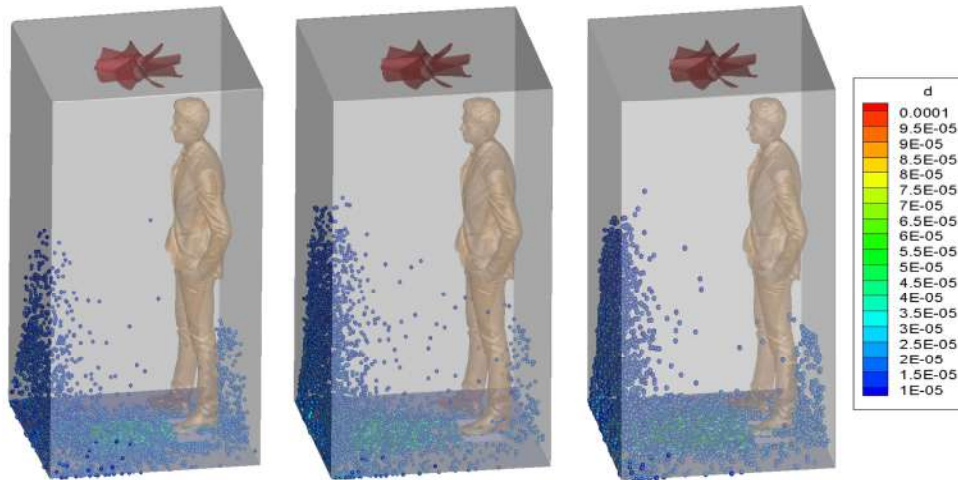
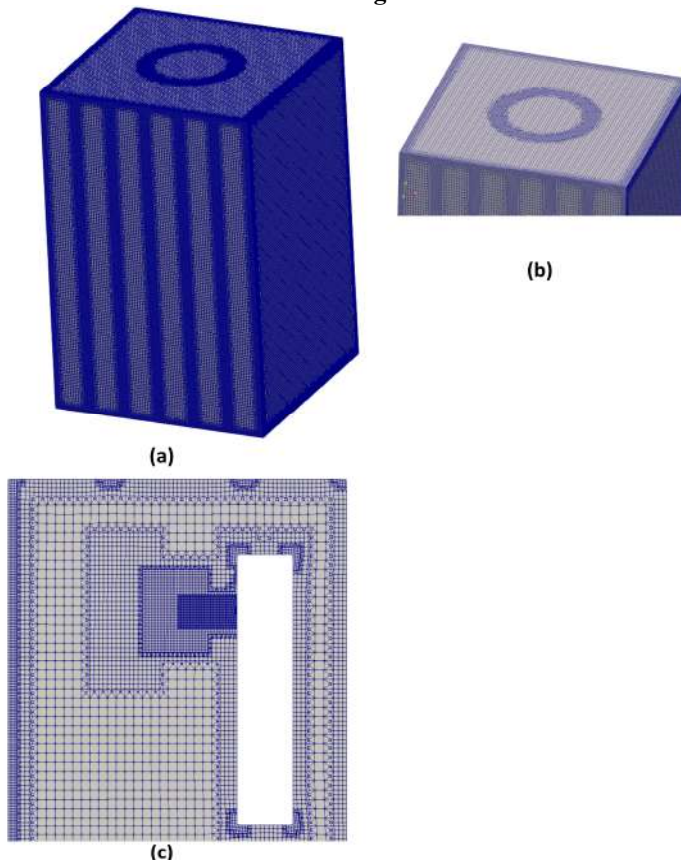


Fig. 4: Comparisons of droplet distributions for coarse, medium and fine mesh sizes respectively from left to right.



**Fig. 5: (a) Adopted Mesh
 (b) Refinements at various locations of the adopted mesh
 (c) Mesh Section showing gradual refinement of mesh near mouth of the Passenger**

E. Grid Independence Study

A 3D structured hexahedral-dominant mesh is used for the discretization of our computational domain. The mesh consists of approximately 5.8×10^5 cells. Mesh refinement is applied near the top mounting, outlets as well as other boundaries, but most importantly, sufficient refinement is applied near the passenger's mouth, from which the cough

droplets are injected, to capture the droplet motion accurately. A smooth and gradual transition was also made from the very refined mesh near the mouth to the ambient mesh. A thorough grid independence study was conducted before selecting the above mesh. Three different mesh sizes; coarse (4,54,327 cells), medium (5,78,669 cells), and fine (6,95,027 cells) have been taken. The Eulerian field velocity U_y is taken as the parameter, against which the results of the 3 different mesh are compared in Fig. 3 (b). The axial velocity (U_y) profile is taken along a line AB of 0.6 m length, the line AB being parallel to the X-axis. The line AB is situated on the plane CD. The plane CD is parallel to the elevator's floor and is at a height of 1 m above the elevator floor. The line AB and the plane CD and their positions inside the elevator domain are shown in Fig. 3 (a). For this purpose of grid independence, scenario 2 (of Table 1) is considered as a representative case. Besides the axial velocity (U_y) profile, the velocity magnitude contours on plane CD and droplet distributions are also compared in Fig. 3 (c) and Fig. 4 respectively. From Figs. 3 (b), 3 (c) and 4, it can be seen that the results of the coarse mesh vary considerably from that of the medium and fine mesh and that the results of the medium and fine mesh have negligible difference. Since results become virtually grid independent with the medium and fine meshes, we adopted the medium mesh for our study. From this, it can be concluded that the medium mesh size considered here is sufficient to capture the flow field correctly inside the elevator. Figure 5 (a) and 5 (b) show our finally adopted 3D mesh of 5,78,669 cells encapsulating the refinement near the boundaries and edges. Figure 5 (c) is showing a section of this mesh which portrays the gradual refinement near the mouth.

III. Validation

I. Validation of Droplet Evaporation Model Including Salt Model

Many previous studies have been conducted but the authors did not consider the effect of soluble components present in the cough droplets. In reality, cough droplets are not pure water and contain dissolved salts (like NaCl) in certain proportions. This presence of salts in cough droplets affects the droplet characteristics in several interconnected ways, as discussed in the Introduction section. In our study, an attempt is being made to make the simulations more realistic by considering the effect of salt solution in cough droplets i.e. by including the salt model of droplets. Our model is tested against the reported experimental result of change of diameter of an acoustically levitated 1 wt% salt (NaCl) laden droplet with time of Basu et al.³⁵. For this validation study, only 1 droplet (NaCl 1% by wt., H₂O 99% by wt.) is injected with initial size of 600 μm at the centre of a domain. To model the quiescent conditions, the domain is taken much larger than the droplet diameter and the internal field as well as the boundary fields of the entire computational domain is assigned a zero velocity. A temperature of 30°C or 303K and a relative humidity of 50% is used as reported by Basu et al.³⁵. In order to model the levitating droplet, the droplet is injected with zero initial velocity and no force (gravitational, buoyancy or sphere drag) is applied on the droplet, thus keeping it suspended in the domain indefinitely. The droplet diameter reduces continuously owing to its evaporation and the change in diameter (D) with time is noted. Fig. 6 (a) compares experimental data (Basu et al.³⁵) of the temporal history of the instantaneous normalized droplet diameter (D/D_0 ; D_0 initial diameter) with our numerically predicted results. The numerically predicted results are in a reasonably good agreement with the experimental observations of Basu et al.³⁵, as can be seen from the two graphs in Fig. 6 (a). Hence our newly developed droplet salt model is validated.

II. CFD Model Validation

Before proceeding with the numerical model for our actual study, a qualitative validation of the droplet dispersion in the domain is done using our salt model against the droplet dispersion reported by Sen¹⁹. The validation data used are that of Scenario 3 of Sen¹⁹. For this validation study, the geometry and all the initial and boundary conditions are that of Scenario 3 of Sen¹⁹. The droplet dispersion pattern as predicted by our numerical (CFD) model is compared with the droplet dispersion results of Scenario 3 of Sen¹⁹. Figure 6 (b) shows the droplet dispersion pattern for the two cases, at two different time instants of $t = 0.27\text{s}$ and $t = 2.27\text{s}$, the left one is the reported result of Sen¹⁹ and the right one is our numerically predicted result.

The match between the droplet dispersion pattern for the two cases is reasonably good, for both time instants. The small deviations that occur can be attributed to the fact that unlike our case the salt water mixture for modelling of the saliva droplets was not implemented by Sen¹⁹. Apart from this, both the cases are in an overall qualitative agreement

(in terms of droplet position at different time instants.) Thus, our numerical (CFD) model is validated and hence, our numerical (CFD) model along with our newly developed salt model can be used subsequently in our actual study.

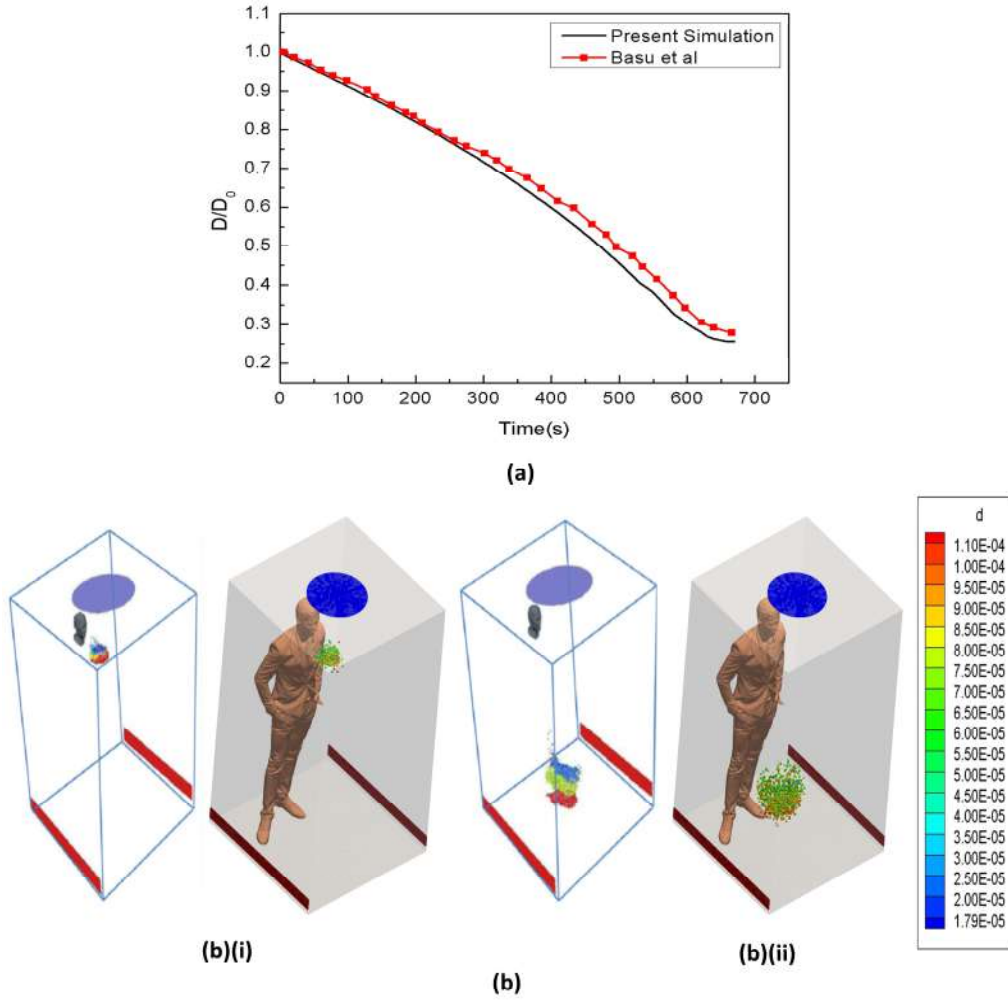


Fig. 6: (a) Validation of droplet evaporation model including crystallisation with literature data (b) Validation of Droplet Dispersion with literature data (left : Sen¹⁹, right: present work) at $t = 0.27s$ ((b)(i)) and $t = 2.27s$ ((b)(ii)) respectively.

Table 1: Table of Scenarios, *\hat{j} indicates positive y direction.			
Scenario	Objective	Axial Velocity of top circular mounting (m/s)	Angular Velocity of top circular mounting (rpm)
1	Effect of quiescent environment	0	0
2	Effect of Axial Inlet	$-0.56\hat{j}$	0
3	Effect of Inlet Fan	$-0.56\hat{j}$	$-2000\hat{j}$
4	Effect of Axial Exhaust	$0.56\hat{j}$	0
5	Effect of Exhaust Fan	$0.56\hat{j}$	$2000\hat{j}$
6	Effect of Door Open (Extension of Scenario 3)	$-0.56\hat{j}$ upto $t = 7s$; 0 after $t = 7s$	$-2000\hat{j}$ upto $t = 7s$; 0 after $t = 7s$

IV. RESULTS AND DISCUSSIONS

In this study six different types of ventilation scenarios, as summarized in Table 1, have been studied. In scenario 1, the effect of a quiescent environment (i.e. no airflow or ventilation condition) is studied. In scenario 2, the effect of an inward axial jet ventilation condition is studied. In scenario 3, the effect of a rotating fan ventilation condition is studied. In scenario 4, the effect of an outward (exhaust) axial jet ventilation condition is studied. In scenario 5, the effect of an exhaust fan ventilation condition is studied. In scenario 6, the effect of the opening of the elevator door i.e. the effect of an increased ventilation area is studied. These scenarios have been studied and quantified (quantifications done after all the 4 cough streams have been injected into the domain) to progressively move towards a ventilation system that minimizes the chances of getting infected for a passenger/passengers if they had been travelling in the elevator (or is waiting outside to enter the elevator) with the above mentioned infected passenger considered in the study.

In Scenario 1, the effect of a quiescent environment on droplet dynamics and heat transfer characteristics have been studied whereas scenarios 2-5 investigate the effect of forced circulation on the same. Scenario 6 is an extension of scenario 3 where we try to find out the changes in droplet dynamics and reduction of risk of getting infected brought out by the opening and closing of the elevator doors.

The choice of ambient temperature 30°C and relative humidity 50%, is typical of a warm and humid day in a tropical country like India. The scenarios 1-5 have been investigated for 10 seconds, the average time taken by an elevator to traverse 10 floors, considering average height of a floor as 3 metres (complying with National Building Code of India, 2005)³⁷ and mean elevator speed as 3 m/s.

A. Transport and Evaporation of Droplets

1. Scenario I

In this scenario, the top mounting is treated as a wall, with no airflow interaction with the domain, thus making a quiescent environment prevail inside the domain. Here, the droplets do not reach the floor within the stipulated elevator travel time of 10 seconds, as established by Fig. 7 (a-e). It is important to note that droplets do not directly head towards the floor rather they get entrapped in the turbulence induced both by the cough and the continuous inhalation and exhalation of the passenger, and they get spread across the elevator. The absence of any continuous draft of air in the domain slows down the process of sticking or escaping of the droplets, hence majority of them remain suspended in the air. The suspended droplets evaporate continuously to decrease in size as visible from the continuous shrinking size range, depicted by the diameter distribution of the suspended droplets at various time instances in Fig. 7 (f-j). Fig. 7 (f-j) also show the droplet nuclei (in red colour). Droplet nuclei are the droplets from which the volatile liquid component has completely evaporated and is remaining only with the nonvolatile salt component. Due to the initial droplet size distribution following a Rosin-Rammler distribution, we have droplet nuclei of different sizes (Fig. 7 (f-j)) and also it is possible to have a droplet and a droplet nuclei of same size (Fig. 7 (f-j)). In this context, it is notable that out of a droplet and a droplet nuclei of same size, the droplet nuclei is more harmful as it has surely been inherited from an initially larger size droplet, thus exhibiting a very high viral load. Also the droplet nuclei basically consist of only the nonvolatile component, which in turn contains the pathogen. A significant number of suspended droplets evaporate to form droplet nuclei having size mostly in the range of 10-20 μm after 10s as shown in Fig. 7 (j).

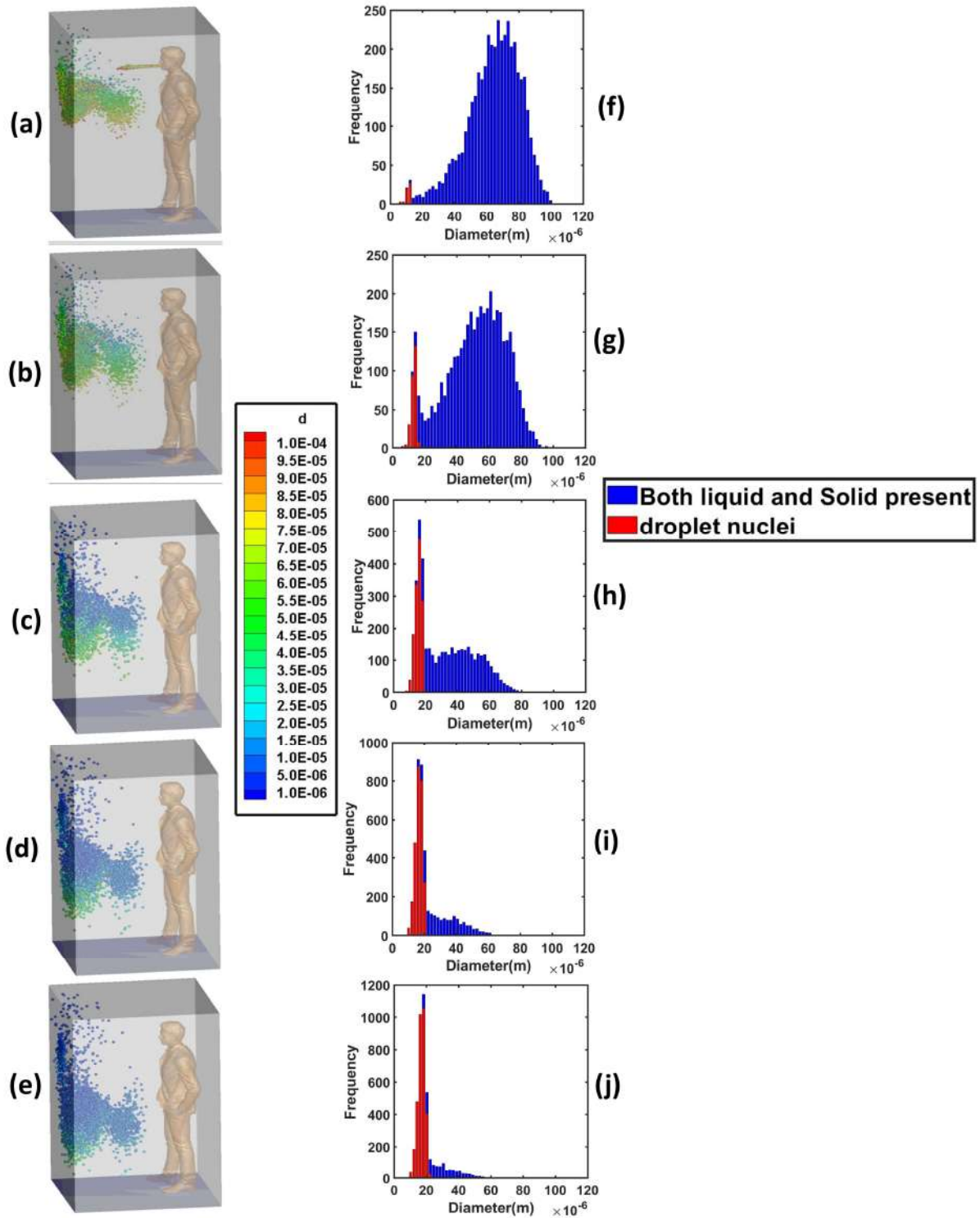


Fig. 7: (a-e) Droplet distribution at 4.14s, 5.5s, 7.48s, 9s, 10s respectively, of Scenario 1. (Man has been shown for illustration purpose only)
(f-j) Corresponding diameter distribution of the suspended droplets at same time instances of 4.14s, 5.5s, 7.48s, 9s, 10s respectively, of Scenario 1.

2. Scenario II

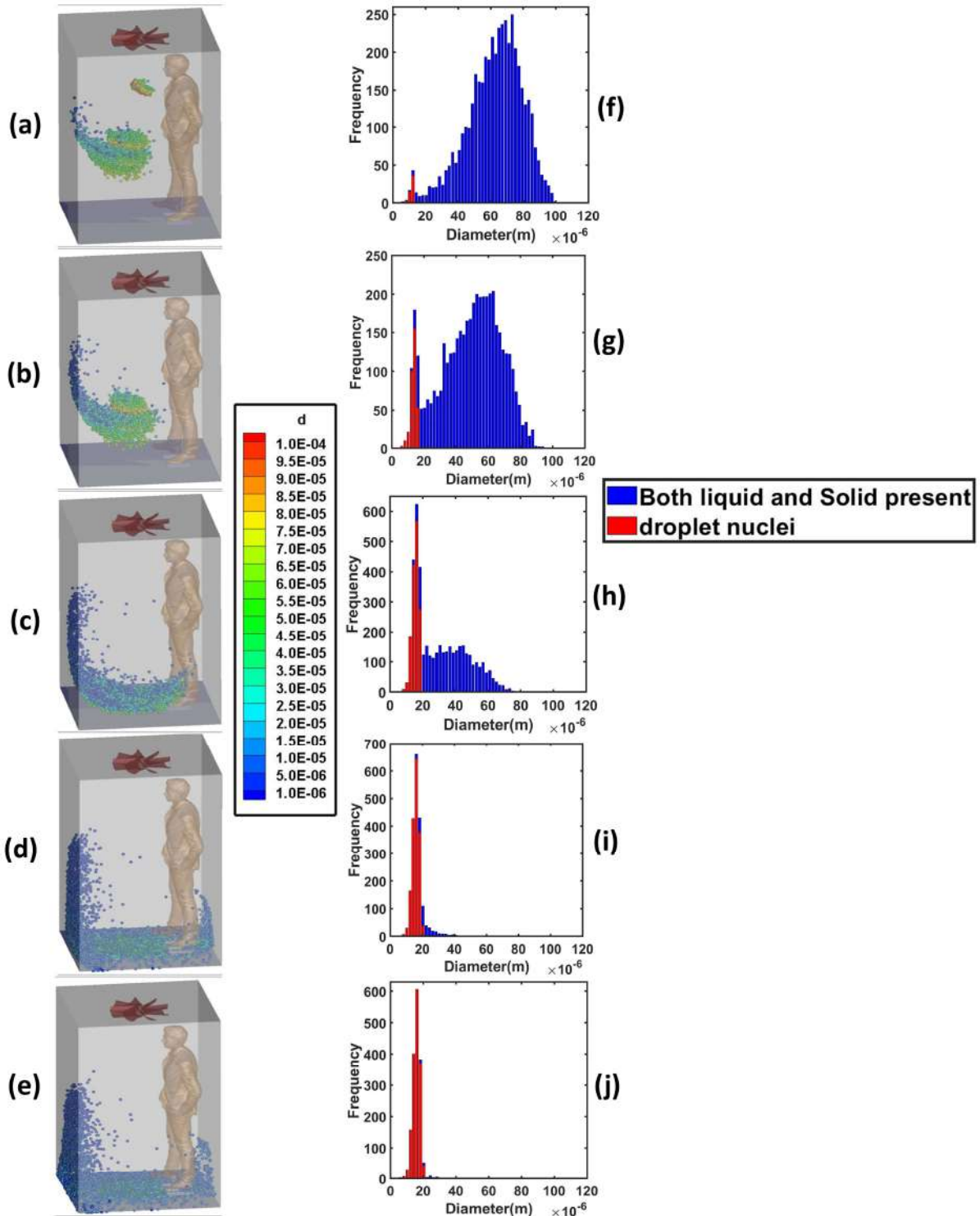


Fig. 8: (a-e) Droplet Distribution at 4.14s, 5.5s, 7.48s, 9s, 10s respectively, of scenario 2.
 (Man and Fan have been shown for illustration purpose only).
 (f-j) Corresponding diameter distribution of the suspended droplets at same time instances of 4.14s,
 5.5s, 7.48s, 9s, 10s respectively, of scenario 2.

In this scenario, the effect of forced circulation is studied by providing a downward axial jet at the top mounting. A comparison of droplet distributions in Fig.8 (a-e) and Fig.7 (a-e) highlights the impact of forced circulation on droplet dynamics. The presence of a strong downward axial flow drives the droplets downwards causing majority of them to reach and stick at the floor very quickly within the stipulated time of 10 seconds. A very small fraction of the droplets goes wayward due to the effect of turbulence puff as discussed in the above scenario. The suspended droplets evaporate continuously to decrease in size as visible from the continuous shrinking diameter range of the diameter distributions of the suspended droplets, depicted at various time instances by Fig. 8 (f-j) while almost all the suspended droplets become droplet nuclei (having size in the range of 10-20 μm) after 10s as shown in Fig. 8 (j).

3. Scenario III

In this scenario, the top mounting is modelled closely as a fan by consideration of its rotational effect. Besides maintaining a strong axial flow, the rotational effect of the fan brings about distinguished changes in the droplet kinematics. The droplet distributions depicted in Fig. 9 (a-e) portray the effect that the rotational effect of fan has brought out in droplet dynamics. The droplets initially move upward upon injection, after being trapped in local vortices, developed in the flow domain near the mouth of the passenger as depicted in the velocity vector plot of Fig. 11, which shows the velocity vectors at a cross-sectional mid-plane AB. The plane AB is perpendicular to the X direction and is situated midway between the two elevator side walls. The orientation and the location of the plane AB inside the elevator domain is shown in Fig. 10. Fig. 11 shows the velocity vectors contoured by temperature, thus also giving an idea of the temperature prevailing inside the domain.

After traversing the vortex (as vindicated by Fig. 11), the particles again come down and get spread across the domain. The rotational effect increases the dispersion in motion due to additional turbulence created by the rotational component of the fan due to which particles spread away randomly to different far-off directions, thus significantly increasing the fraction of particles stuck at the various surfaces of the elevator and hence decreasing the fraction of suspended particles in the domain as can be understood from the droplet distributions depicted at various time instances by Fig. 9 (a-e). The suspended droplets evaporate continuously to decrease in size as visible from the continuous shrinking diameter range of the diameter distributions of the suspended droplets, depicted at various time instances by Fig. 9 (f-j) while maximum suspended droplets turn into droplet nuclei (having size in the range of 10-20 μm) after 10s as shown in Fig. 9 (j).

4. Scenario IV

All the forced circulation scenarios investigated leading up to this scenario involved enforcing air into the domain. In this scenario air is drawn out of the domain and the top mounting is modelled as an axial exhaust jet. As can be seen from the droplet distribution (Fig. 12 (a-e)), the elevator space (mostly the upper portion) is filled with many suspended particles. This is due to the fact that the first two streams of cough particles move down instead of moving up, while the third and fourth ones move up. This difference occurs because the flow has not developed during the time of injection of first two streams as depicted by the velocity contours at plane AB (plane AB shown in Fig. 10) of different time instances in Fig. 14, where the development of velocity in the flow field along with the droplets' positions have been depicted. As the flow takes sufficient time to develop as reconfirmed by the temperature contoured velocity vector plots at plane AB (Fig. 13), the initially injected particles do not receive sufficient drag force to move upwards hence descends (due to gravity), but as the flow becomes fully developed, the downward motion of the particles get arrested and these particles remain suspended in the domain for an extended period of time. As air is drawn out in this scenario, a significant percentage of droplets escape out of the domain. Also it may be noted here that particles either escape or remain suspended, but as seen from Fig. 12 (a-e), particles do not stick at different elevator surfaces, unlike the previous scenarios. The suspended droplets evaporate continuously to decrease in size as indicated by the continuous decreasing diameter range of the diameter distributions of the suspended droplets, depicted at various time steps by Fig. 12 (f-j) while majority of the suspended droplets turn into droplet nuclei (having size in the range of 10-20 μm) after 10s as shown in Fig. 12 (j).

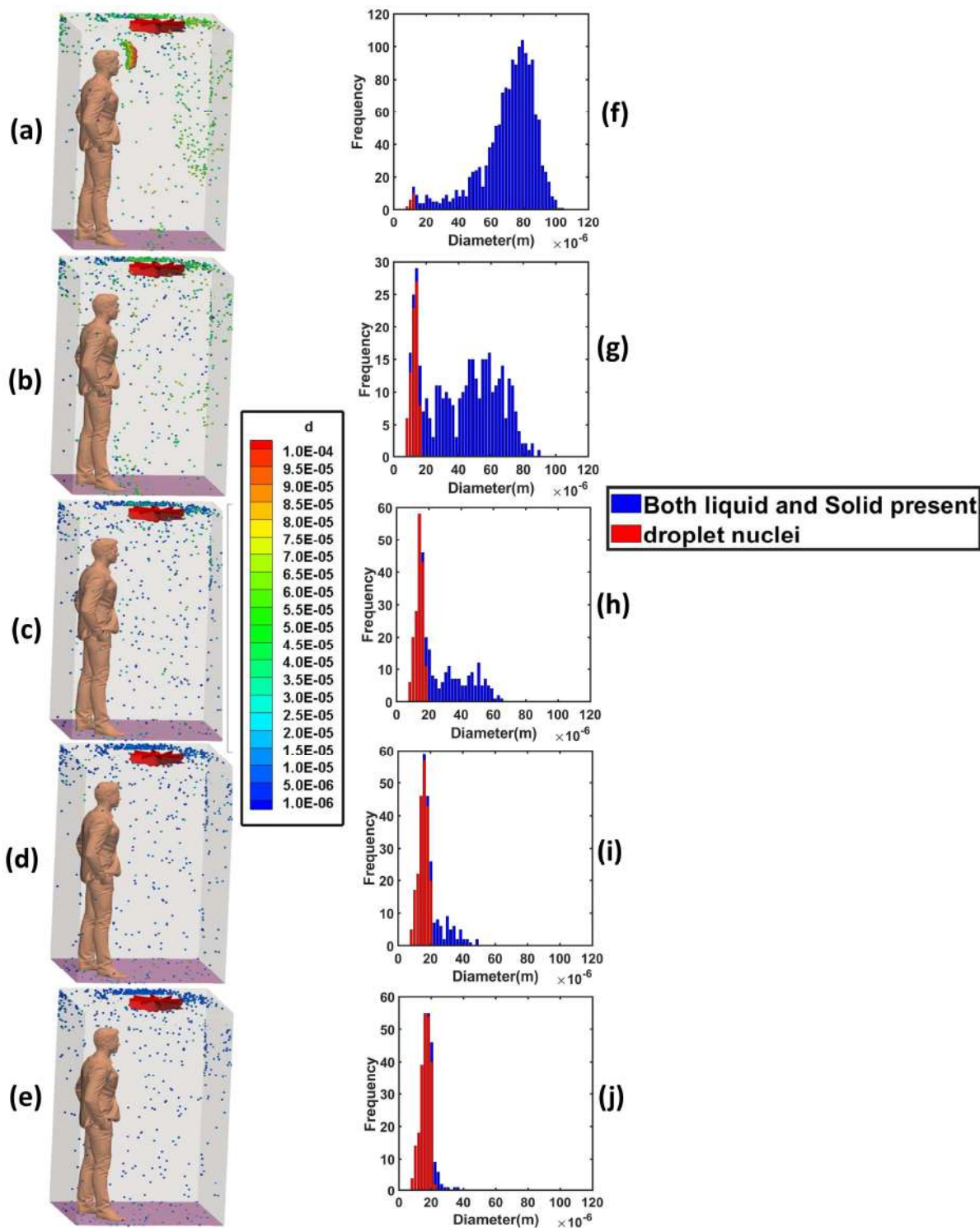


Fig. 9: (a-e) Droplet Distribution at 4.14s, 5.5s, 7.48s, 9s, 10s respectively, of scenario 3. (Man and Fan have been shown for illustration purpose only). (f-j) Corresponding diameter distribution of the suspended droplets at same time instances of 4.14s, 5.5s, 7.48s, 9s, 10s respectively, of scenario 3.

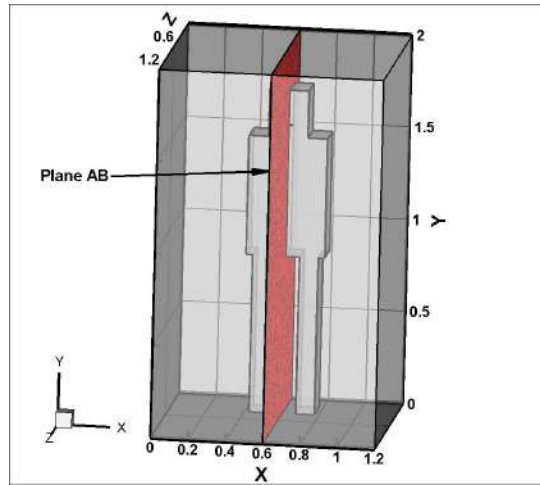


Fig. 10: Showing cross-sectional plane AB .

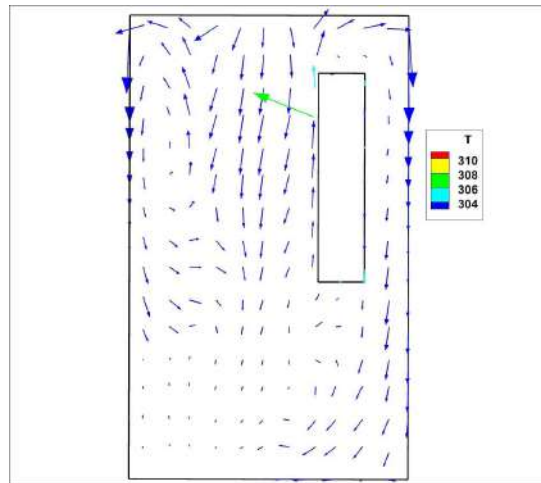


Fig. 11: Velocity Vector Plot at plane AB (of Fig. 10), of Scenario 3.

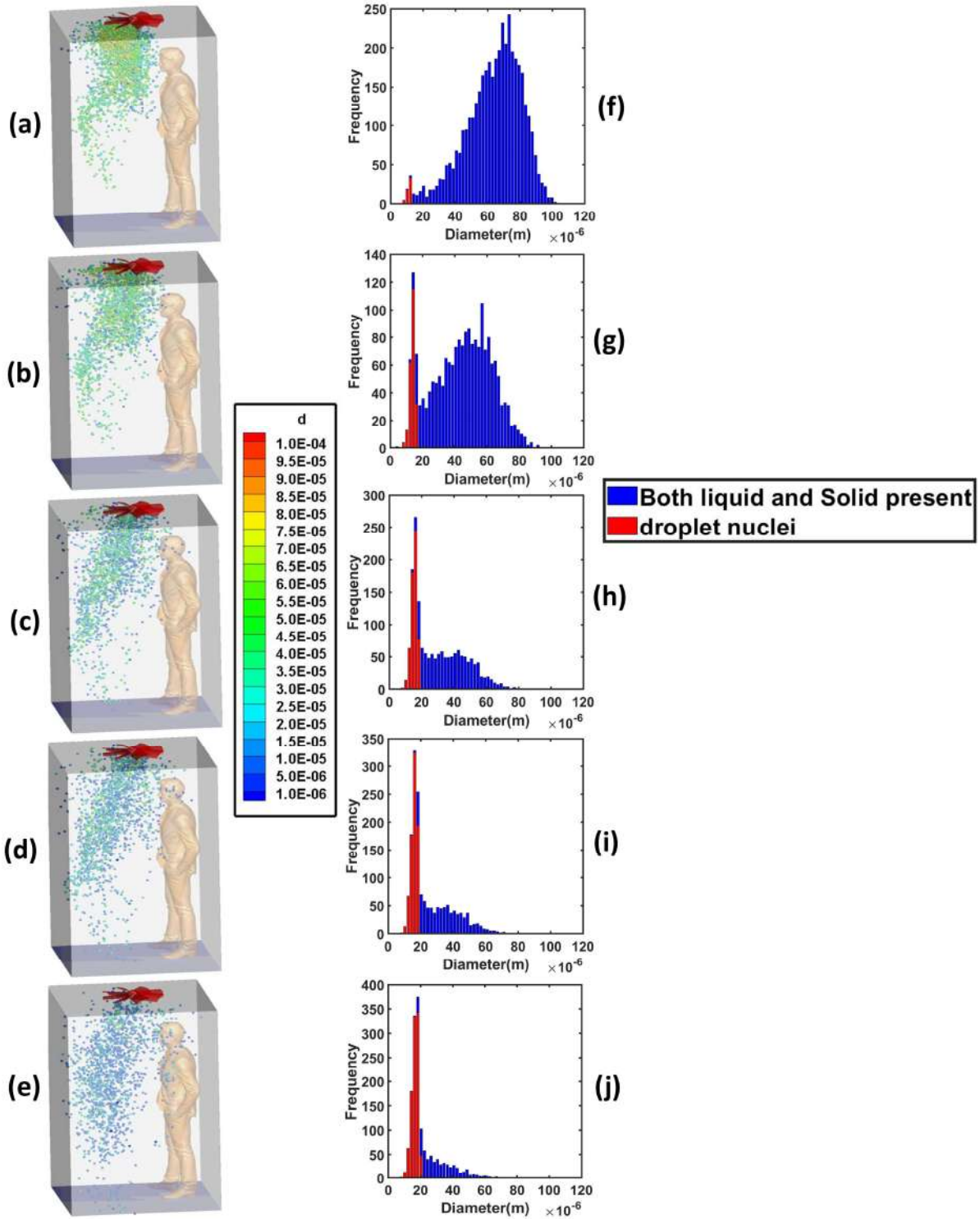


Fig. 12: (a-e) Droplet Distribution at 4.14s, 5.5s, 7.48s, 9s, 10s respectively, of scenario 4. (Man and Fan have been shown for illustration purpose only). (f-j) Corresponding diameter distribution of the suspended droplets at same time instances of 4.14s, 5.5s, 7.48s, 9s, 10s respectively, of scenario 4.

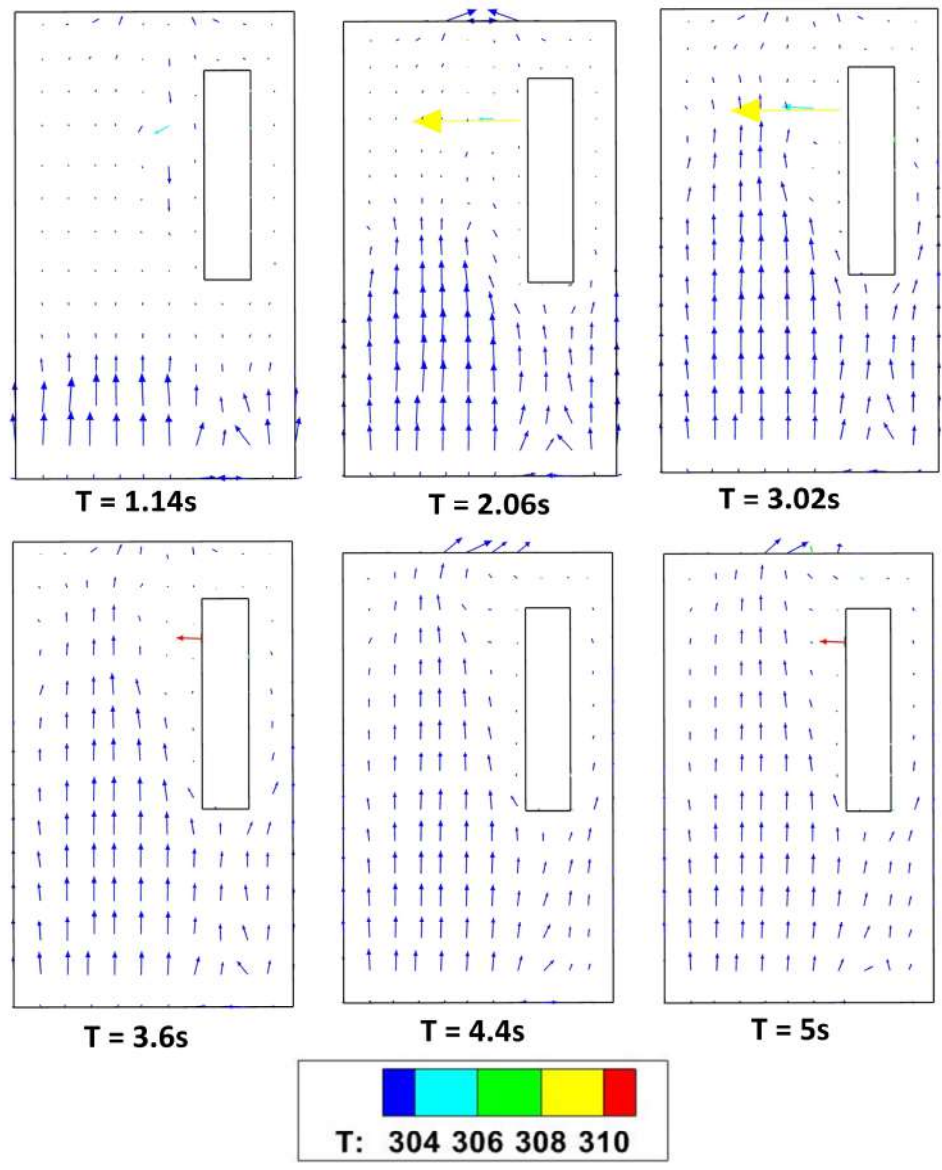


Fig. 13: Velocity vector plots at plane AB (of Fig. 10) at different time instances, of scenario 4.

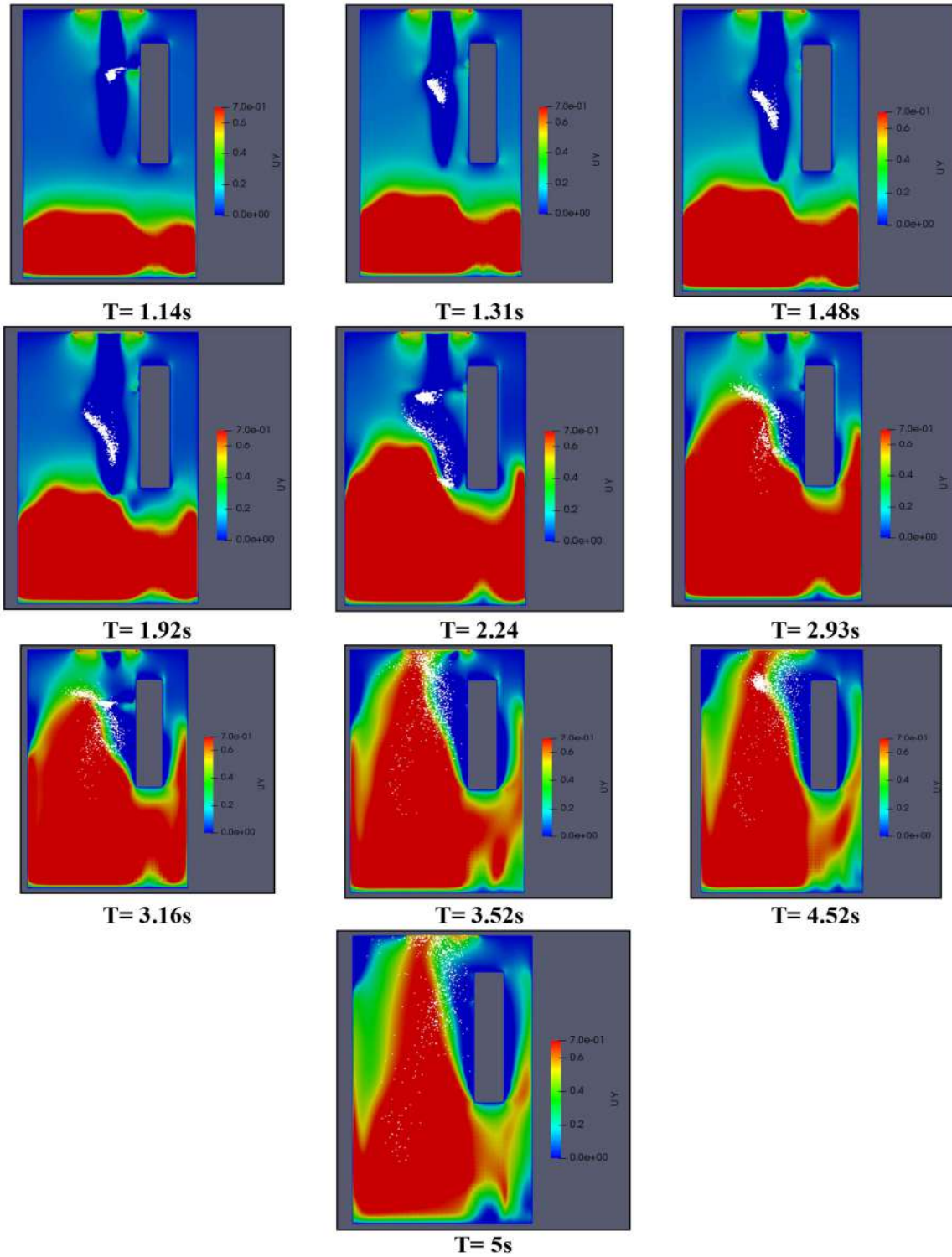


Fig. 14: Velocity contours at plane AB (of Fig. 10) along with droplets, at various instances of Scenario 4.

5.Scenario V

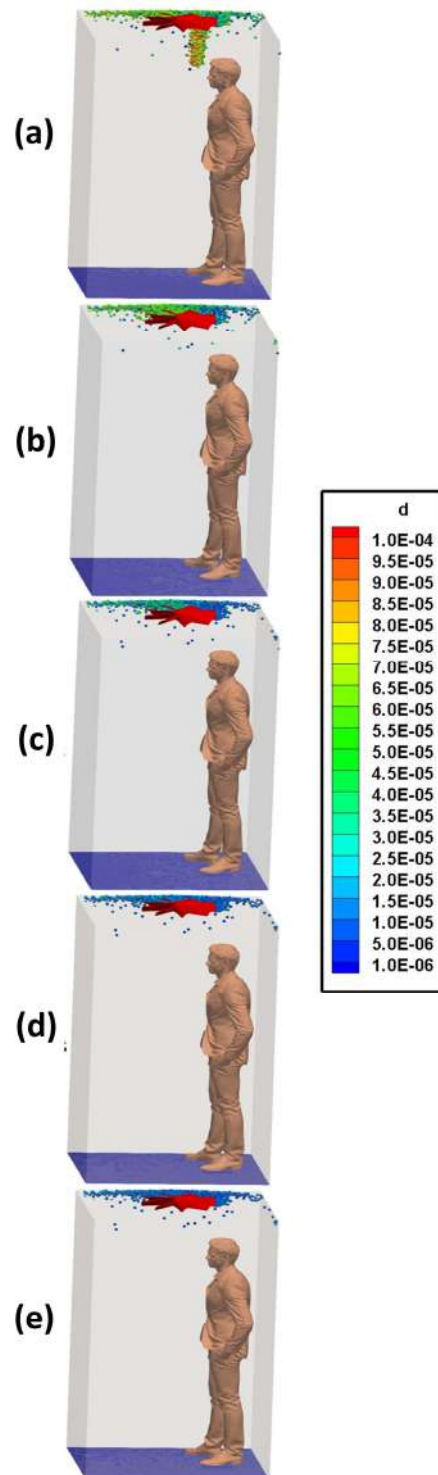


Fig. 15: (a-e) Droplet Distribution at 4.14s, 5.5s,7.48s,9s,10s respectively, of scenario 5.

Just like scenario III of rotating fan, in this scenario, the top mounting is modelled as an exhaust fan considering its rotation. Unlike the previous scenario, the flow develops rather quickly in the domain and the particles move upwards immediately upon injection due to the more enhanced drag force exerted by air on the particles, as can be seen from

the droplet dispersion transience depicted in Fig. 15 (a-e). The circulation brought about by the rotational effect, increases the dispersion in droplet kinematics due to the additional turbulence (created by the rotating component of the fan), due to which the droplets rise up and a significant amount of them gets deposited at the roof (top wall) of the elevator, quite contrary to the previous scenario of axial exhaust jet. As can be understood from the droplet distribution in Fig. 15 (a-e), after 5.5 s, none of the droplets remain below the height of the passenger. Hence the domain becomes completely safe from this time instant.

6. Scenario VI

This scenario is an extension of the third scenario, where the doors of the elevator has been gradually opened, following which the passenger left the elevator, after which the door was closed gradually. The opening of the door began at 4.14 seconds and continued till 6 seconds. The door had remained open till 9 seconds and was completely closed at 10.5 seconds. The fan was switched off at 7 seconds and the passenger had left the domain at 7 seconds. The opening, closing and stall time was maintained following the ASME A 17.1 safety guidelines for Elevators and Escalators³⁸. The motivation for this investigation is two-fold. Firstly, it was intended to comprehend the time required for an elevator to be deemed safe after an infected passenger had left the domain following the injection of droplets. Secondly, this scenario leads to the understanding of the droplet dynamics in the domain when there is a significant increase in ventilation area. As can be seen from the droplet distributions of Fig. 16 (a-d) and Fig. 17 (a-d), the opening of doors with the fan being kept on, expedites the particle escape process. But, once the fan is switched off there is hardly any change in the number of droplets escaping from the domain as there is no enforcing flow to do so. As the fan is switched off and door is closed there is a significant decrease in flow strength in the subsequent time instances with the air becoming almost stagnant after a certain duration in the domain. The small number of droplets which remain suspended in the domain after closing the door, will remain indefinitely suspended thereafter, as the air has become almost stagnant in the domain which can be understood from the droplet distribution figures of Fig. 16 (a-d) and Fig. 17 (a-d). The suspended droplets evaporate continuously to decrease in size as visible from the continuous shrinking diameter range of the diameter distributions of the suspended droplets depicted at various time instances by Fig. 16 (e-h) and Fig. 17 (e-h) while all the droplets become droplet nuclei (having size in the range of 10-22 μm) within 38s as shown in Fig. 17 (g).

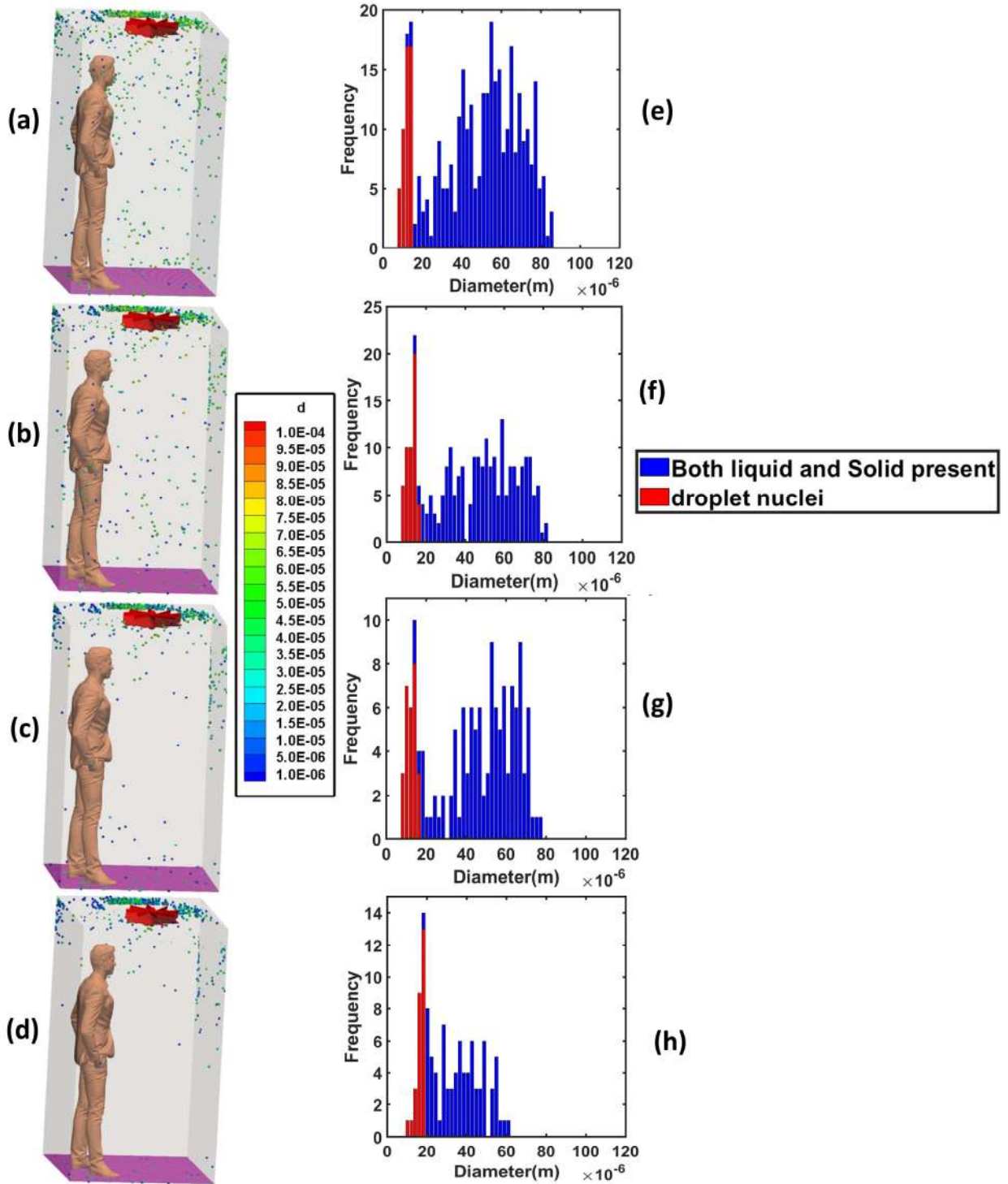


Fig. 16: (a-d) Droplet Distribution at 4.80s, 5.33s,6s,7s respectively, of scenario 6.
(e-h) Corresponding diameter distribution of the suspended droplets at same time instances of 4.80s, 5.33s,6s,7s respectively, of scenario 6.

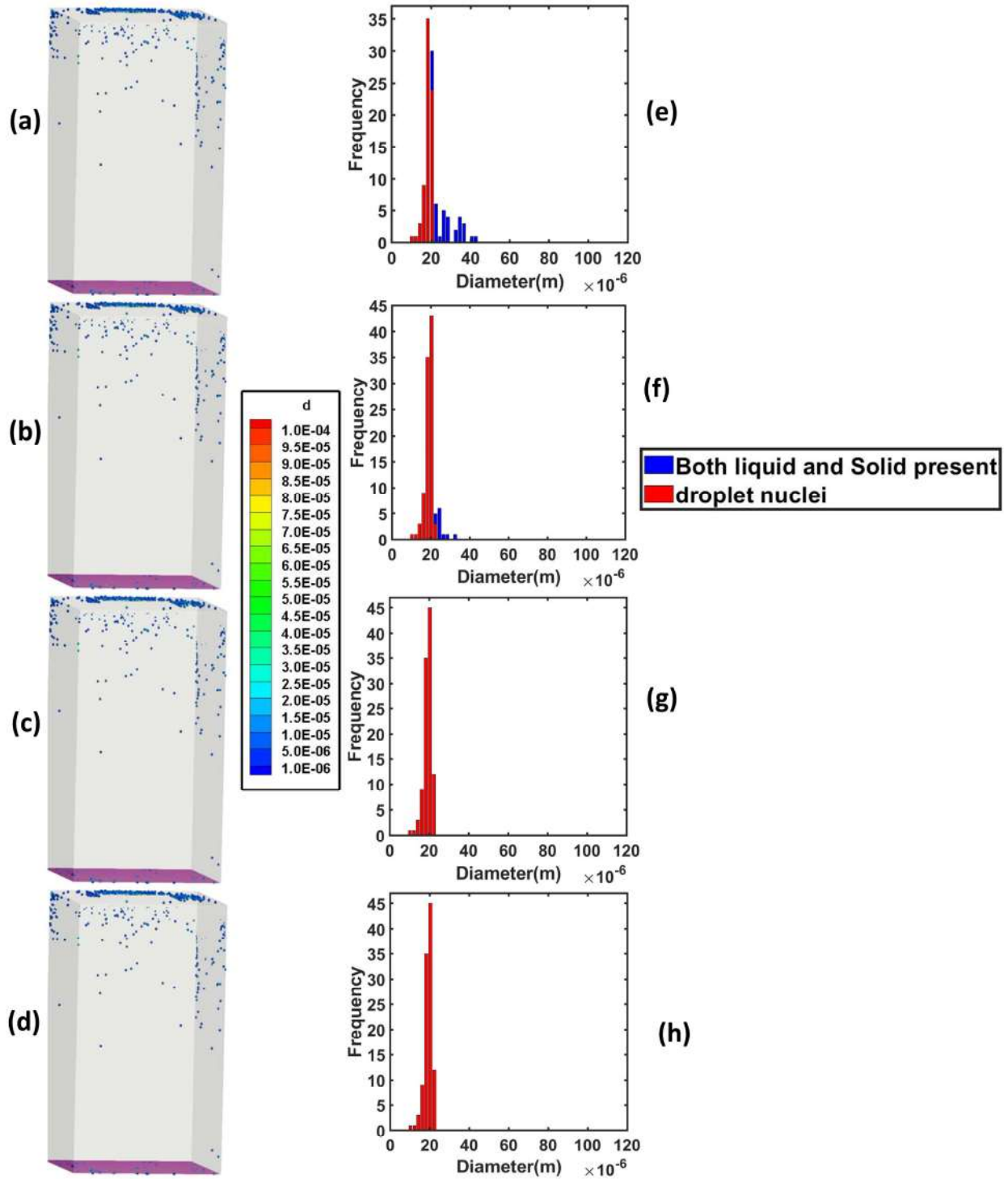


Fig. 17: (a-d) Droplet Distribution at 9s, 10.5s,38,95.56s respectively, of scenario 6.
 (e-h) Corresponding diameter distribution of the suspended droplets at same time instances of 9s,
 10.5s,38,95.56s respectively, of scenario 6.

B. Implications for Spread of Disease

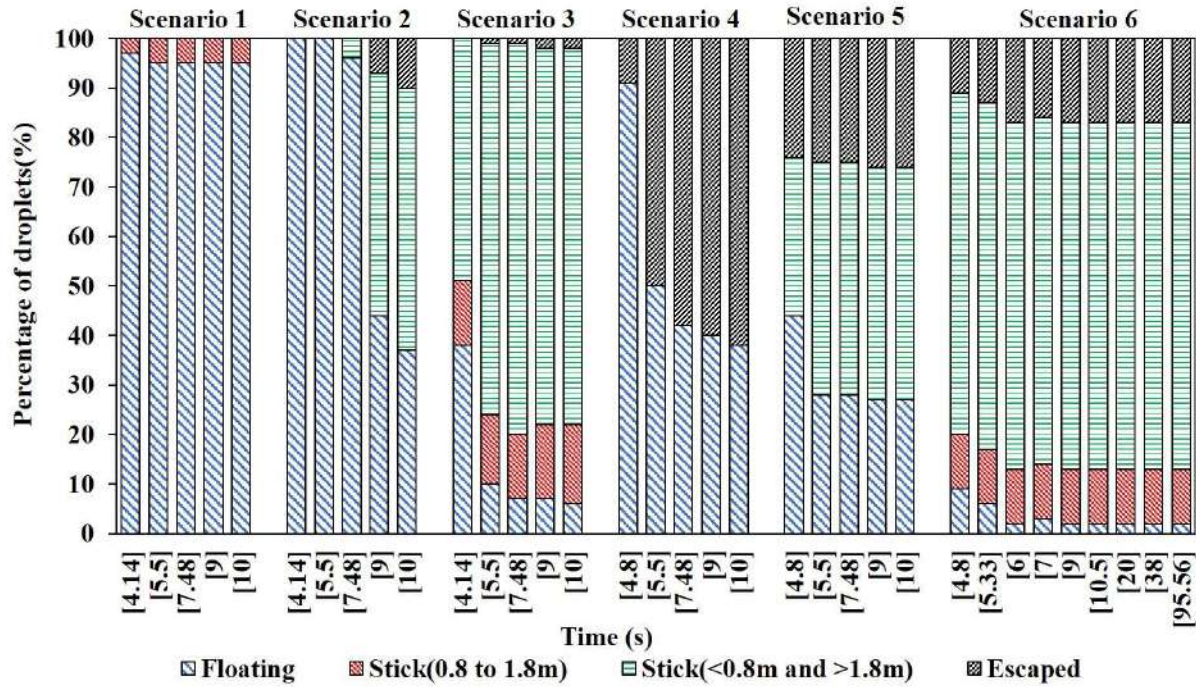


Fig. 18: Showing droplet fate at various time instants for all the scenarios.

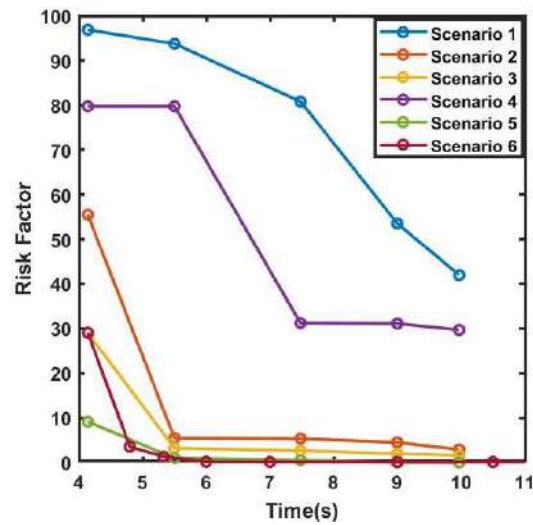


Fig. 19: Showing risk factor (percentage of suspended droplets in the range of 0.8m to 1.8m) at various time instances for various scenarios.

Time Instants	No. of Droplets in risky height zone
4.8	143
5.33	58
7	6
10.5	4
95	4

Table 2: Droplets remaining suspended in the risky height zone at different time instances of scenario 6.

It is a critically acclaimed fact that the two main modes of spread of coronavirus are by touch and inhalation of particles having significant viral load. So, it is critical that we investigate how the dispersed droplets in the domain might come in contact with a person and obtain a better understanding on this aspect. At first it is important to quantify how the droplets disperse in the domain by enumerating the percentage of injected droplets that remains suspended in the domain, that escapes from the domain and the percentage that gets deposited on the elevator surfaces. The height range 0.8m to 1.8m, (average height from a person's waist to head) is identified as the risky height zone as droplets (either suspended or deposited on surfaces) in this zone will be most perilous to any other person travelling in the elevator as these droplets may be directly inhaled by the other passengers. Fig. 18 shows the percentage of injected droplets that remains suspended in the domain, the percentage that escapes and the percentage of droplets that gets deposited within and outside the risky height zone on the elevator surfaces, for the various scenarios. A parameter called Risk Factor is defined as the percentage of injected particles that remains suspended in the domain within the risky height zone and this parameter is an indicator of the probability of an exposed passenger to get infected. This risk factor has been depicted at different time instants for the different scenarios in Fig. 19. It is understood from Fig. 18 and Fig. 19, that in a quiescent domain where there is no continuous draft of air, almost all the droplets remain suspended in the domain and only a few percentage gets deposited on surfaces. Also a fair percentage of suspended droplets remains in the risky height zone at all times (Fig. 19), thus producing the highest risk factor of all the scenarios, rendering a bleak future to the elevator and its other passengers. But the introduction of a forced circulation of air in the domain alleviates this problem and produces a significant change in droplet dynamics, as can be seen from Fig. 18, by significantly reducing the percentage of droplets that remains suspended in the domain and increasing the percentage of droplets that either gets deposited on the elevator surfaces or escapes out of the domain. In scenario 2, there is an orderly movement of air in the axially downward direction which causes all the droplets to initially remain suspended in the risky height zone, but the presence of a forced circulation expedites the downward movement of droplets causing the majority of droplets to get deposited on the floor (approximately 50% at 10s) and a small percentage to escape out through the outlets (approximately 10% at 10s) at later time instants thus bringing down the risk factor considerably. For scenario 3, where the modelling of a fan has been done by considering its rotational effect, the situation improves significantly from scenario 2. The increased dispersion in the domain, due to the additional turbulence created by the rotating component of the fan significantly decreases the percentage of droplets that remains suspended in the domain and also in the risky height zone at all times as compared to scenario 2, thus exhibiting a significantly lower risk factor at all instances, as vindicated by Fig. 19. Also the increased dispersion in the domain contributes to increase in the percentage of droplets getting deposited on the elevator surfaces at various locations. In scenario 4 and 5, air is drawn out of the domain. From the risk factor graph (Fig. 19), it is quite evident that compared to other forced circulation scenarios, scenario 4 has significantly greater risk factor at all instants of time (but lesser than the quiescent scenario). This is due to the fact that during the first two cough streams, flow has not developed in the domain and they remain suspended in the domain as discussed earlier, thus producing a significantly higher risk factor at all instants. As air is drawn out of the domain in this scenario, out of all the scenarios, the percentage of injected droplets that escapes out of the domain is greatest, as can be seen in Fig. 18. So in scenario 4, air is drawn out, a considerable amount of droplets also escapes, but still this Scenario offers a high risk factor. Just like scenario 3, the exhaust fan situation has been modelled in scenario 5, considering the rotational effect of fan. Also it is important to note that as the droplets move continuously upward upon injection, after 5.5s no droplets remain in the risky height zone thus causing the risk factor to become zero from this instant onwards. Just like scenario 4, due to the suction effect of air, a significant percentage of droplets escapes out of the domain but there is a difference. In scenario 4, air is drawn axially outward due to which particles escape freely through the top mounting without being stuck at the top wall, but in scenario 5, the additional turbulence created by the rotational effect of the fan also causes a significant amount of particles to get deposited at the roof (top wall) of the elevator alongside causing some particles to escape. Also the drop in risk factor from scenario 4 to scenario 5 is much more than the drop from scenario 2 to scenario 3. This difference is attributed to the higher risk factor of scenario 4 as compared to scenario 2 (risk factors of scenario 3 and scenario 5 being more or less same). In scenario 2, there is an axially downward flow of air, and droplets have an inherent tendency to drop down due to the effect of gravity. The two effects assist each other and the droplets essentially precipitate downwards due to the two conducive effects, decreasing the number of suspended droplets in the risky height zone, thus reducing the risk factor. On the other hand, in scenario 4, initially the effect of gravity is predominant due to which droplets tend to come down but this phenomenon is ephemeral, and after some time, when the flow develops, the droplets come under the influence of two opposing forces of similar order of magnitude, causing these droplets to remain levitated

suspended in the domain (mainly in the risky height zone), thus maintaining a high risk factor throughout. Also in scenario 4, due to absence of enhanced dispersion and additional turbulence (created by the rotating component of a fan) and the droplet movement being ordered, there is no mechanism to make the droplets stick at the elevator surfaces and hence the droplets remain floating inside the elevator – another potent reason for such a high risk factor. Scenario 6 is an extension of scenario 3 where the doors are opened and closed. Due to a huge increase in ventilation area, the percentage of droplets escaping out of the domain is significantly higher compared to the scenarios where the air is enforced into the domain (Scenarios 2 and 3). As discussed earlier, it is evident from Fig. 18, after the fan has been switched off (at 7s), percentage of droplets that have escaped from the domain does not increase any more. The percentage of droplets that remain deposited on the elevator surface does not change much from scenario 3. Due to increase in escape percentage of droplets, the percentage of droplets that remain suspended in the domain (also in the risky height zone as indicated by risk factor plot of Fig. 19) decreases significantly compared to scenario 3. Also the number of droplets remaining suspended in the risky height zone decreases quickly with time (indicated by Table 2) reducing to only 4 droplets being suspended at 10.5 seconds, hence it can be irrefutably concluded that within 3.5 seconds of abeyance, the elevator has become completely safe and can be used again without any intimidation.

Till now we have emphatically established the fact that out of all the ventilation scenarios, scenario 5 is the best case scenario as after sometime there remains no droplet in the risky height zone making the domain completely safe. But it is also important to note that if any of the scenarios are being used as ventilation condition in an elevator, the safe radial distances to be maintained from the mouth of the infected passenger to ensure maximum safety in the elevator must also be investigated. Hence, firstly height of each suspended droplet in the domain has been tracked at the end of 10s (20s, 38s and 95s for scenario 6) as shown in Fig. 20 (a-c) and Fig. 21 (a-c) and secondly, among these suspended droplets, the radial distance of those droplets suspended in the risky height zone has been tracked, as depicted in Fig. 20 (d-f) and Fig. 21 (d-e) in order to ascertain the minimum radial distance to be maintained in all the cases to avoid as much as possible, coming in contact with any droplet in the risky height zone. The safe distances for all scenarios are enumerated in the table below (Table 3). The domain for scenarios 5 and 6 (there are only 4 droplets in the risky height zone at 4 discrete locations in scenario 6, as seen in Fig. 21 (e)) are completely safe. Out of the remaining scenarios, the quiescent scenario requires to maintain the maximum radial distance (1.1312 m) from the passenger's mouth to get rid of the palpable danger pervading the elevator domain.

Another important fact that was investigated was the rate of evaporation of the suspended droplets in the domain – indicated by the rate of formation of droplet nuclei from the suspended droplets. It is important to understand that these droplets will continuously evaporate to form very small-sized particles that will remain suspended in air for a very long duration and will have a high chance of infecting any other person travelling in the elevator. Figure 22 shown below depicts the percentage of suspended droplets that have fully evaporated to form droplet nuclei at different time instances for various scenarios. It can be seen for all forced circulation scenarios except for scenario 4, the evaporation rate is higher than that of quiescent scenario (scenario 1). This is due to the fact that in the forced circulation scenarios, the increased velocity of the droplets increases the evaporation rate owing to the increased Sherwood number for the droplets. But in scenario 4, the evaporation rate is slower compared to the other scenarios because it takes significant amount of time for the flow to develop and droplet cloud from the first two streams travel together in a cluster remaining condensed (and suspended) rather than spreading across the domain hence residing in areas having locally higher concentration of water vapour, thereby slowing the evaporation rate. Still we can say that a significant fraction of suspended droplets gets fully evaporated to droplet nuclei very quickly. This is due to low concentration of water vapour in the domain owing to low value of relative humidity (30%) which leads to a high evaporation rate. This high evaporation rate is a matter of concern, as a significant percentage of injected droplets quickly evaporates to form virusols, i.e. particles having very high viral load and diameter less than 20 μ m which remain suspended in the domain for a long period of time³⁹. These virusols are the most dangerous of all the droplets. Because of their size (dia<20 μ m), they have the highest penetration in human lungs⁴⁰. A comparison of the percentage of injected droplets that have formed suspended virusols in the risky height zone at different time instants is shown in Fig. 23 below. As expected, the forced circulation scenarios except scenario 4 have very small fractions of virusols due to overall decrease in the percentage of suspended particles. In scenarios 1 and 4, albeit the rate of evaporation being less (Fig. 22), but the increased percentage of suspended droplets in the risky height zone, as discussed earlier, contributes to the formation of virusols in this zone, thus increasing the percentage of virusols in the risky height zone, as depicted in Fig. 23. Scenario 1 has the highest concentration of virusols suspended in the risky height zone (Fig.

23), thus aggravating the threat of infection inside the elevator. Fig. 24 (a-c) and Fig. 25 (a-b) portray the size ranges of the droplets suspended in the risky height zone, thus giving an idea of the viral load residing in this regime and it also tracks the droplets' radial locations and their concentration in a single plot, for scenarios 1, 2, 3, 4 and 6 respectively. Fig. 24 (d-f) and Fig. 25 (c-d) extracts out the virusols and shows separately the radial concentration of these virusols suspended in the risky height zone i.e. the number of virusols suspended at different radial locations from the mouth and thus give an idea of the most critical radial distance i.e. the radial distance having the highest concentration of malicious virusols. The most critical (or the most dangerous) radial distance for the different scenarios is enumerated in Table 4. This most critical radial distance must always be eluded by the other passengers to somewhat avert the chances of infection.

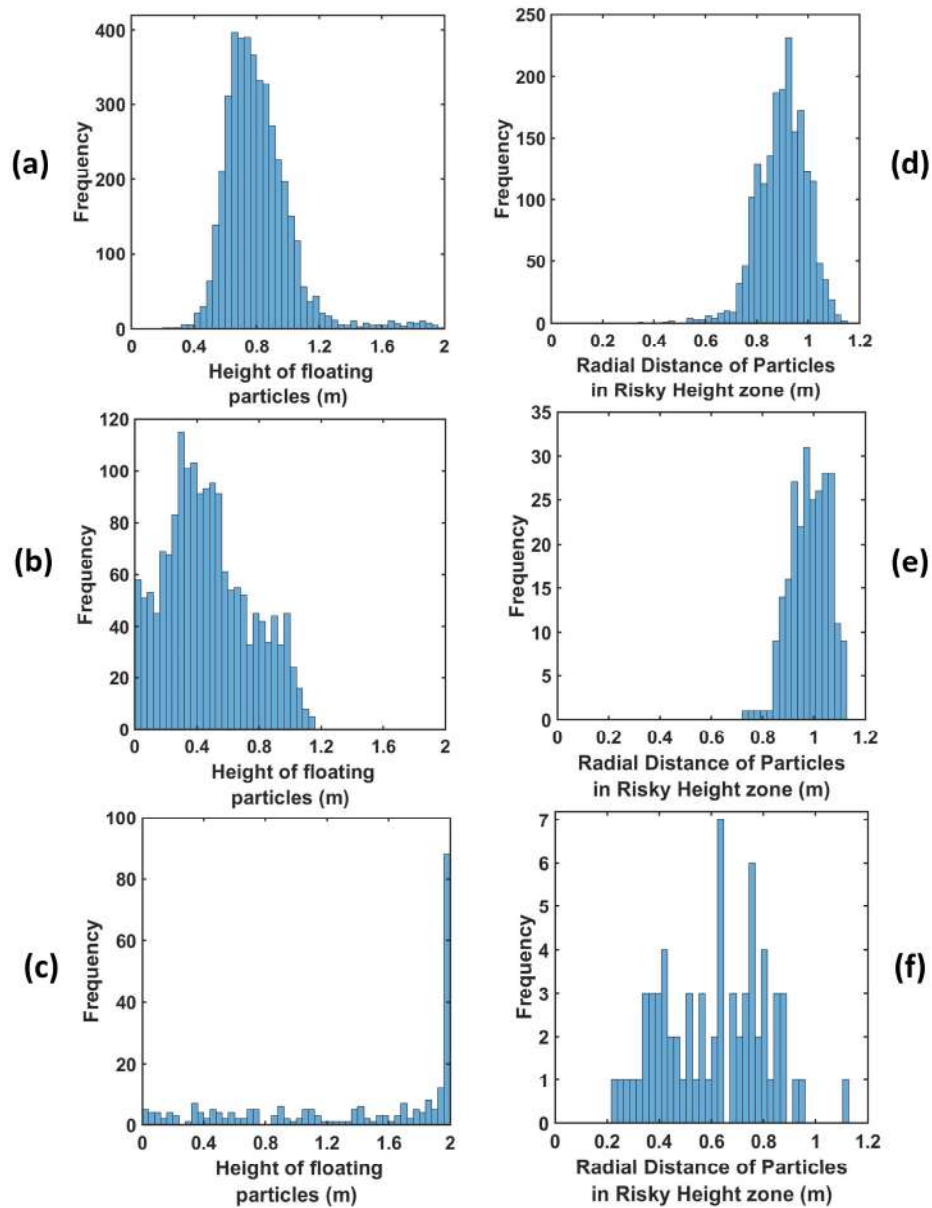


Fig. 20: (a-c) showing height distribution of suspended particles for scenarios 1, 2 and 3 respectively at the end of 10s.

(d-f) showing radial distance distribution in risky height zone for scenarios 1, 2 and 3 respectively at the end of 10s.

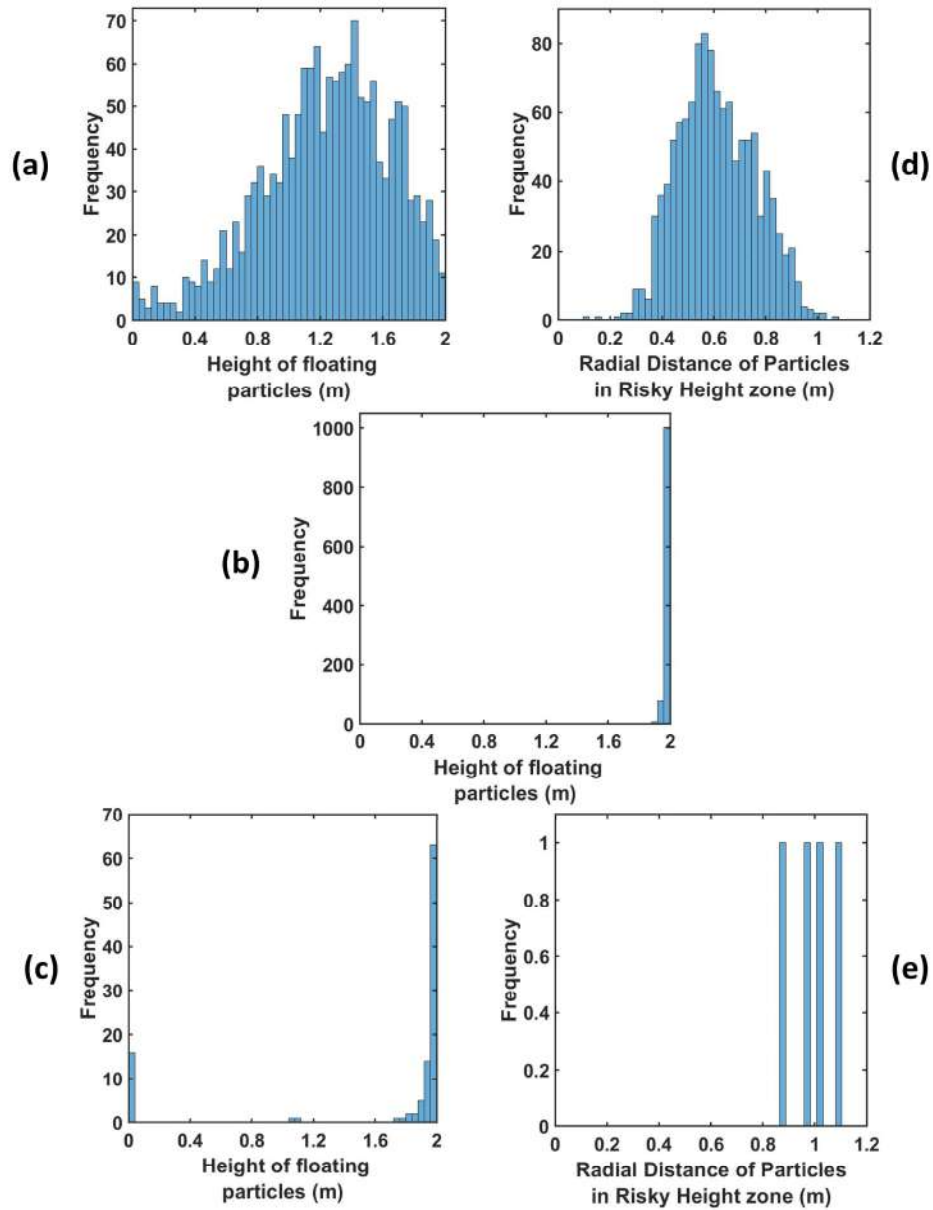


Fig. 21: (a-c) showing height distribution of suspended particles for scenarios 4, 5 and 6* respectively at the end of 10s.

(d-e) showing radial distance distribution in risky height zone for scenarios 4 and 6* respectively at the end of 10s.

*For scenario 6 it is at the end of 20s, 38s, 95s.

Scenarios	Distance (m)
Scenario 1	1.1312
Scenario 2	1.1184
Scenario 3	1.13
Scenario 4	1.0682
Scenario 5	Entire Domain is Safe
Scenario 6	Entire Domain is Safe

Table 3: Table showing safe radial distances for various scenarios.

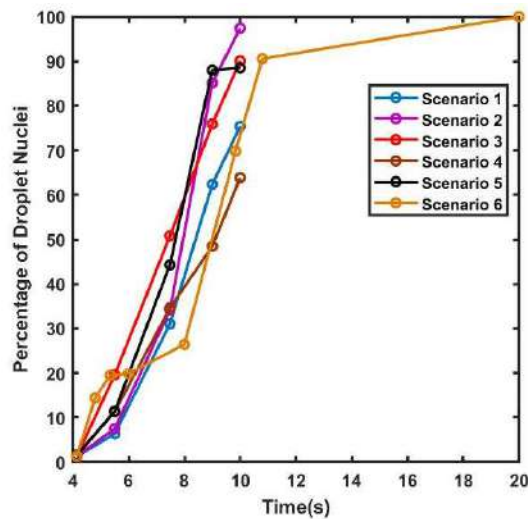


Fig. 22: Percentage of suspended droplets that have fully evaporated to droplet nuclei at different time instances for various scenarios.

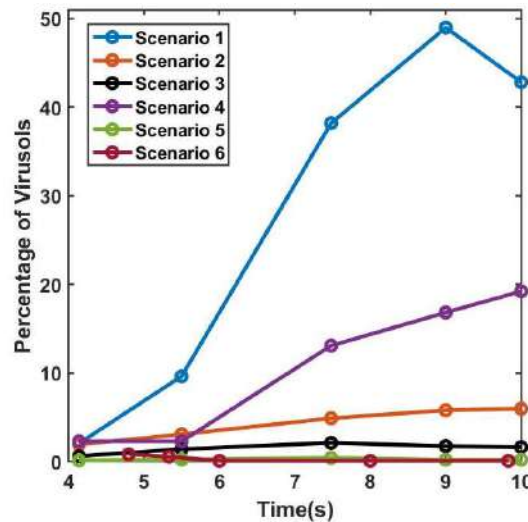


Fig. 23: Percentage of suspended virusols in the risky height zone at different time instances for various scenarios.

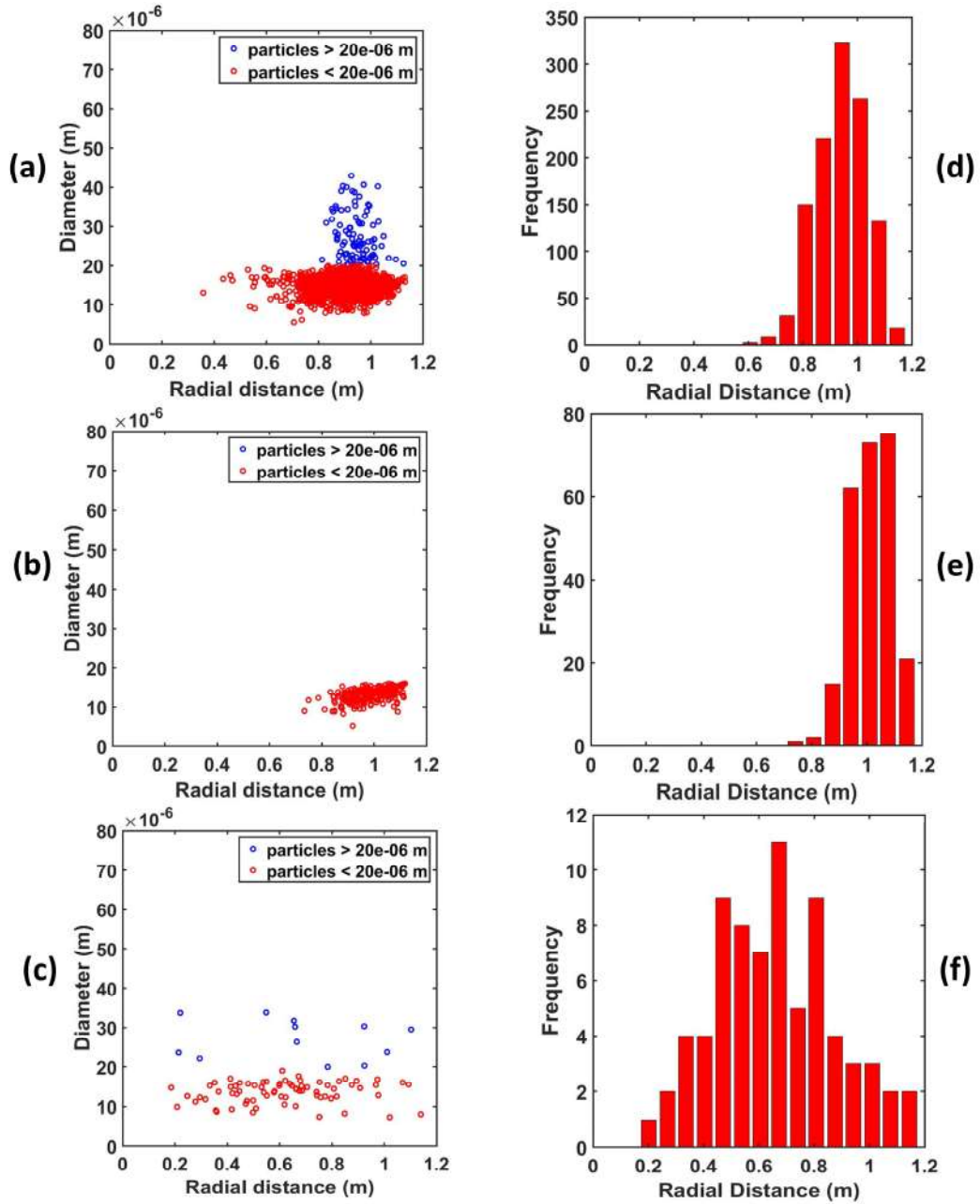


Fig. 24: (a-c) showing radial location tracking and diameter of the suspended particles in the risky height zone after 10s, for scenarios 1, 2 and 3 respectively. (d-f) showing radial distribution of virusols suspended in the risky height zone after 10s, for Scenarios 1, 2 and 3 respectively.

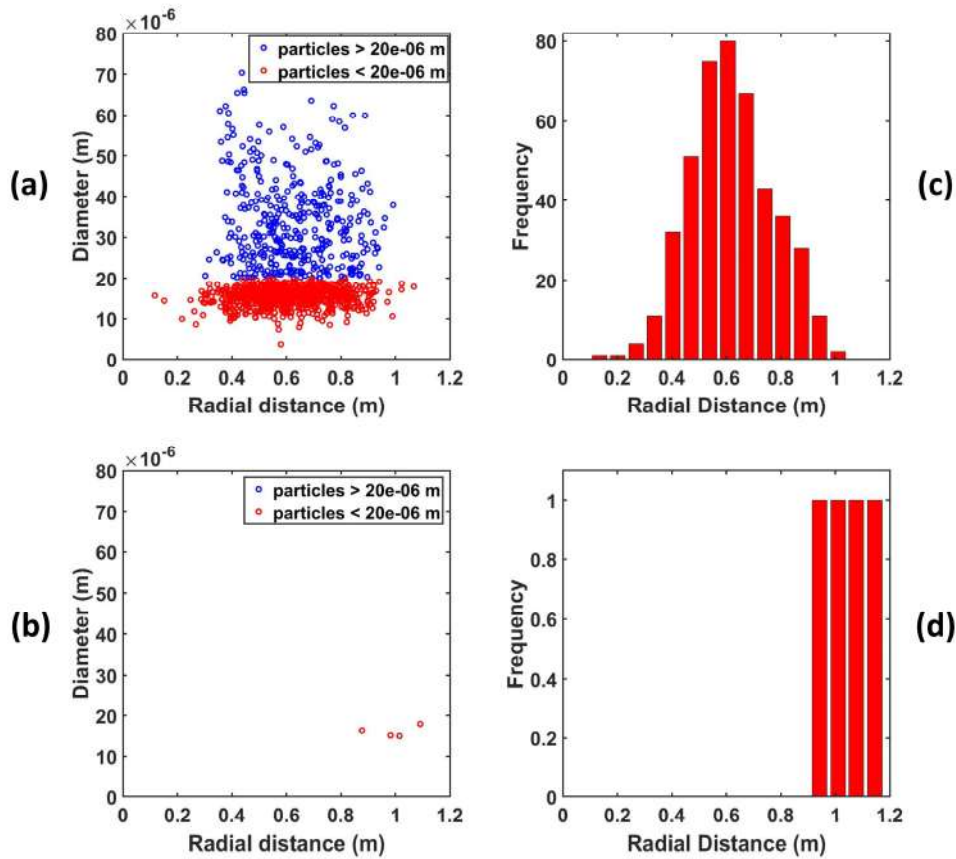


Fig. 25: (a-b) showing radial location tracking and diameter of the suspended particles in the risky height zone for scenario 4 (after 10s) and for scenario 6 (after 10.5s,20s,95.56s) respectively. (c-d) showing radial distribution of virusols suspended in the risky height zone for Scenario 4 (after 10s) and for scenario 6 (after 10.5s,20s,95.56s) respectively.

Scenarios	Distance (m)
Scenario 1	0.95
Scenario 2	1.1
Scenario 3	0.65
Scenario 4	0.6
Scenario 5	Entire Domain is Safe
Scenario 6	Entire Domain is Safe

Table 4: Table showing the most critical radial distance for various scenarios.

V. CONCLUSION

The transmission and evaporation of injected droplets in the domain has been modelled by a 3D Eulerian-Lagrangian numerical model. An elevator, usually used in multi-storeyed residential or small enterprise buildings have been modelled. Various ventilation scenarios within the elevator have been simulated. As the droplets move according to the prevailing ventilation patterns, their evaporation is affected by prevailing air, velocity, temperature and humidity. In these investigations various scenarios have been explored to understand the droplet dynamics in the domain.

The simulation results show that, a quiescent condition in the elevator has a very high risk associated with it as significantly large percentage of droplets remain suspended in the domain in the risky height zone (0.8m to 1.8m).

But as long as there is forced circulation in the domain, much lesser percentage of droplets remain suspended in the domain. Either they get stuck on the elevator surfaces or escape from the domain. Thus, the presence of a forced circulation is necessary to expedite either the escaping or sticking process of the particles. In all the ventilation scenarios having a continuous draft of air, a maximum of 29.68% and minimum of 0% of injected droplets remain suspended in the air, whereas for the quiescent scenario, the corresponding percentage is 42.01%. The high percentage of suspended droplets and the high risk factor in the quiescent condition is an indictment of the poor ventilation in such an elevator, thus clearly depicting the indispensability of ventilation or forced circulation in an elevator to curb the transmission and spreading of virus. Out of all the forced circulation scenarios, implementing an exhaust fan (scenario 5) renders the elevator completely safe (risk factor 0%) (risk factor is defined as the percentage of injected droplets that remain suspended in the domain) within a short period of time. It also has been found that in general maintaining a minimum distance (from the passenger's mouth) of around 1.1m ensures complete safety.

Although the forced circulation ventilation scenarios mitigate risk factor significantly than the quiescent scenario, in general, for forced circulation scenarios, the increased air velocity expedites the evaporation process of the droplets (caused by an increase in Sherwood number) also the increase in turbulence of flow causing dispersion of droplets into areas having lesser mass fraction of water vapour also contributes to the increased evaporation rate. The increased evaporation rate increases the percentage of virusols among the suspended droplets. These virusols (diameter $< 20\mu\text{m}$), besides having very high viral loading also have the largest penetration in human trachea. The most critical radial distance (i.e. the radial distance having the highest concentration of virusols) for various scenarios is also obtained from our study. Other fellow passengers inside the elevator must always try to avoid this critical radial distance. The increased evaporation rate also causes larger percentage of suspended droplets in the domain to get converted to droplet nuclei compared to the quiescent ventilation condition.

It is important to understand, that the scenarios that have been simulated in this study are just a fraction of many likely real life scenarios in which the dimensions of the elevator, air supply and outflow slots, location of a fan or exhaust fan, velocity and speed, total time of elevator travel may be different from what are considered in this study. The passenger height and his/ her positions inside the elevator may also vary. The results are expected to be significant to these parametric variations and some of these scenarios may pose significant threat in addition to the ones shown. Thus, it is advised to take utmost precautionary measures while using an elevator.

NOMENCLATURE	
C_p	Specific heat capacity of Eulerian phase (air) ($\text{Jkg}^{-1}\text{K}^{-1}$)
$C_{p,d}$	Specific heat capacity of droplet ($\text{Jkg}^{-1}\text{K}^{-1}$)
C_d	Coefficient of drag
d_d	Diameter of droplet (m)
D_{eff}	Effective diffusivity (m^2s^{-1})
D_{mol}	Molecular diffusivity in air (m^2s^{-1})
F_{lift}	Lift force on droplets(N)
f_v	Mass fraction of water vapour in Eulerian phase
H	Enthalpy (Jkg^{-1})
h	Convective heat transfer coefficient ($\text{Wm}^{-2}\text{K}^{-1}$)
h_{fg}	Latent heat of vaporisation of droplet (Jkg^{-1})
k	Turbulent kinetic energy (Jkg^{-1})
k_t	Thermal conductivity ($\text{Wm}^{-1}\text{K}^{-1}$)
k_{mt}	Mass transfer coefficient for droplet (ms^{-1})
m_d	Mass of droplet (kg)
p	Static pressure of Eulerian phase (Nm^{-2})
P	Turbulent kinetic energy production ($\text{Nm}^{-2}\text{s}^{-1}$)
RH	Relative humidity (percentage)
T	Temperature (K)
T_d	Temperature of droplet (K)
\vec{u}	Velocity of the Eulerian phase (ms^{-1})

\vec{u}_d	Velocity of droplet (ms^{-1})
ρ	Density of Eulerian phase (kgm^{-3})
Y_d^s	Mass fraction of nonvolatile component of droplet
Y_d^l	Mass fraction of volatile component of droplet
ρ_d	Density of droplet (kgm^{-3})
m_d^0	Initial mass of droplet (kg)
$C_{p,s}$	Specific heat capacity of nonvolatile component of droplet ($\text{Jkg}^{-1}\text{K}^{-1}$)
$C_{p,l}$	Specific heat capacity of volatile component of droplet ($\text{Jkg}^{-1}\text{K}^{-1}$)
t	Time (s)
μ	Dynamic viscosity of Eulerian phase ($\text{kgm}^{-1}\text{s}^{-1}$)
μ_t	Turbulent viscosity of Eulerian phase ($\text{kgm}^{-1}\text{s}^{-1}$)
Y_0^s	Initial mass fraction of nonvolatile component of droplet
m_{wl}	Molecular wt. of volatile component in droplet(kg)
Sh	Sherwood number
Nu	Nusselt number

References

- ¹ M. Richard, J.M.A. van den Brand, T.M. Bestebroer, P. Lexmond, D. de Meulder, R.A.M. Fouchier, A.C. Lowen, and S. Herfst, *Nat. Commun.* **11**, 1 (2020).
- ² World Health Organization, Geneva World Heal. Organ. 19 (2020).
- ³ L. Bourouiba, E. Dehandschoewercker, and J.W.M. Bush, *J. Fluid Mech.* **745**, 537 (2014).
- ⁴ J. Redrow, S. Mao, I. Celik, J.A. Posada, and Z. gang Feng, *Build. Environ.* **46**, 2042 (2011).
- ⁵ J. Wei and Y. Li, *Build. Environ.* **93**, 86 (2015).
- ⁶ S.B. Kwon, J. Park, J. Jang, Y. Cho, D.S. Park, C. Kim, G.N. Bae, and A. Jang, *Chemosphere* **87**, 1260 (2012).
- ⁷ X. Li, Y. Shang, Y. Yan, L. Yang, and J. Tu, *Build. Environ.* **128**, 68 (2018).
- ⁸ G.R. Johnson, L. Morawska, Z.D. Ristovski, M. Hargreaves, K. Mengersen, C.Y.H. Chao, M.P. Wan, Y. Li, X. Xie, D. Katoshevski, and S. Corbett, *J. Aerosol Sci.* **42**, 839 (2011).
- ⁹ T. Dbouk and D. Drikakis, *Phys. Fluids* **32**, (2020).
- ¹⁰ H. Wang, Z. Li, X. Zhang, L. Zhu, Y. Liu, and S. Wang, *Phys. Fluids* **32**, (2020).
- ¹¹ M.R. Pendar and J.C. Páscoa, *Phys. Fluids* **32**, (2020).
- ¹² Y. Feng, T. Marchal, T. Sperry, and H. Yi, *J. Aerosol Sci.* **147**, (2020).
- ¹³ H. Li, F.Y. Leong, G. Xu, Z. Ge, C.W. Kang, and K.H. Lim, *Phys. Fluids* **32**, (2020).
- ¹⁴ F. Liu, H. Qian, Z. Luo, S. Wang, and X. Zheng, *Build. Environ.* **180**, 106988 (2020).
- ¹⁵ C.H. Cheng, C.L. Chow, and W.K. Chow, *Build. Environ.* **183**, 107196 (2020).
- ¹⁶ X. Yang, C. Ou, H. Yang, L. Liu, T. Song, M. Kang, H. Lin, and J. Hang, *J. Hazard. Mater.* **397**, 122609 (2020).
- ¹⁷ Y. Yan, X. Li, Y. Shang, and J. Tu, *Build. Environ.* **121**, 79 (2017).
- ¹⁸ Y. Yan, X. Li, and J. Tu, *Build. Environ.* **148**, 96 (2019).
- ¹⁹ N. Sen, *Phys. Fluids* **33**, (2021).
- ²⁰ T. Dbouk and D. Drikakis, *Phys. Fluids* **33**, (2021).

- ²¹ A. Agrawal and R. Bhardwaj, *Phys. Fluids* **32**, (2020).
- ²² T. Dbouk and D. Drikakis, *Phys. Fluids* **33**, (2021).
- ²³ T. Dbouk and D. Drikakis, *Phys. Fluids* **32**, (2020).
- ²⁴ S.H. Smith, G.A. Somsen, C. van Rijn, S. Kooij, L. van der Hoek, R.A. Bem, and D. Bonn, *Phys. Fluids* **32**, 107108 (2020).
- ²⁵ K. Ashwini, A.K. Anjali, and V. Sivaswamy, *Int. J. Res. Pharm. Sci.* **11**, 1022 (2020).
- ²⁶ T. Greenhalgh, J.L. Jimenez, K.A. Prather, Z. Tufekci, D. Fisman, and R. Schooley, *Lancet* **397**, 1603 (2021).
- ²⁷ J. Akhtar, A.L. Garcia, L. Saenz, S. Kuravi, F. Shu, and K. Kota, *Phys. Fluids* **32**, (2020).
- ²⁸ T. Dbouk and D. Drikakis, *Phys. Fluids* **32**, (2020).
- ²⁹ EN 81-1:1998 E, Central Secretariat: rue de Stassart 36, B-1050 Brussels, 1998
- ³⁰ Sergio A. Chillón, Ainara Ugarte-Anero, Iñigo Aramendia, Unai Fernandez-Gamiz and Ekaitz Zulueta, *Numerical Modeling of the Spread of Cough Saliva Droplets in a Calm Confined Space*, *Mathematics*, **9(5)**, (2021).
- ³¹ H. Jasak, “OpenFOAM: Open source CFD in research and industry,” *Int. J. Nav. Archit. Ocean Eng.* **1**, 89–94 (2009).
- ³² F. R. Menter, “Two-equation eddy-viscosity turbulence models for engineering applications,” *AIAA J.* **32**, 1598–1605 (1994).
- ³³ W. E. Ranz and W. R. Marshall, “Evaporation from drops. Part I,” *Chem. Eng. Prog.* **48**, 141–146 (1952).
- ³⁴ W. E. Ranz and W. R. Marshall, “Evaporation from drops. Part II,” *Chem. Eng. Prog.* **48**, 173–180 (1952).
- ³⁵ S. Basu, P. Kabi, S. Chaudhuri, A. Saha, Insights on drying and precipitation dynamics of respiratory droplets from the perspective of COVID-19, *Physics of Fluids*, **32(12)**, 2020, p. 123317.
- ³⁶ W. Sutherland, “The viscosity of gases and molecular force,” *Philos. Mag.* **36**, 507–531 (1893).
- ³⁷ National Building Code of India, Bureau of Indian Standards, Manak Bhavan, 9 Bahadur Shah Zafar Marg, New Delhi-110 002, 2005
- ³⁸ ASME A17.1-2010, Safety Code for Elevators and Escalators, The American Society of Mechanical Engineers, Three Park Avenue, New York, NY, 10016 USA
- ³⁹ Christian E. Junge, *International Geophysics*, **4**, (1963).
- ⁴⁰ Antonio F. Miguel, *Medical Engineering and Physics*, **000**, (2017).